Semiclassical Motion of Charge Carriers in Planar Graphene

Bachelor-Arbeit
zur Erlangung des Hochschulgrades
Bachelor of Science
im Bachelor-Studiengang Physik

vorgelegt von

Joris Josiek
geboren am 06.08.2000 in Dresden

Institut für Theoretische Physik
Fakultät Physik
Bereich Mathematik und Naturwissenschaften
Technische Universität Dresden

Abteilung für Theoretische Physik
Helmholtz-Zentrum Dresden-Rossendorf

2021

Eingereicht am 19. Juli 2021

1. Gutachter: Prof. Dr. Ralf Schützhold
2. Gutachter: Prof. Dr. Jan Carl Budich

Abstract

Graphene is a novel two-dimensional material which is attracting much attention due to its unique electronic properties. Notably, electrons moving through graphene lose their effective mass, giving rise to phenomena that can be described in the ultrarelativistic limit of special relativity. This motivates the study of kinematics and dynamics for charged massless particles in electromagnetic fields, even though such particles are not fundamentally predicted by the standard model and none have been observed as free particles. In this work, we review the quantum formalism typically used to describe particles in graphene and then use the WKB approximation to obtain classical equations of motion. We then present ways to examine the semiclassical trajectories of particles in specific examples of electric and magnetic fields. Specifically, we first consider the case of a pure homogeneous magnetic field and then also include a homogeneous electric field. Finally, we investigate the inhomogeneous electric field produced by a hyperbolic tangent potential with a homogeneous magnetic field.

Zusammenfassung

Graphen ist ein neuartiges zwei-dimensionales Material, das aufgrund seiner einzigartigen elektronischen Eigenschaften viel Aufmerksamkeit auf sich zieht. Insbesondere haben Elektronen in Graphen keine effektive Masse, weshalb sich die daraus entstehenden Phänomene im ultrarelativistischen Grenzfall der speziellen Relativitätstheorie betrachten lassen. Dies motiviert die Auseinandersetzung mit Kinematik und Dynamik masseloser geladener Teilchen in elektromagnetischen Feldern, obwohl solche Teilchen im freien Zustand weder vom Standardmodell vorhergesagt noch jemals experimentell beobachtet wurden. In dieser Arbeit resümieren wir den typischen Formalismus, um quantenmechanische Teilchen in Graphen zu beschreiben, und benutzen anschließend die WKB-Näherung um klassische Bewegungsgleichungen zu erhalten. Anschließend präsentieren wir anhand spefizischer Beispiele von elektrischen und magnetischen Felder diverse Methoden, um die quasiklassischen Bahnkurven von Teilchen zu untersuchen. Zuerst betrachten wir ein reines homogenes magnetisches Feld und erweitern dieses dann durch ein homogenes elektrisches Feld. Schließlich untersuchen wir gemeisam mit einem homogenen Magnetfeld noch ein inhomogenes elektrisches Feld, das durch ein Potential in Form eines hyperbolischen Tangens erzeugt wird.

Acknowledgements

I would like to sincerely thank everyone who has made this project possible for me.

First and foremost, my gratitude goes to my advisor Prof. Dr. Ralf Schützhold for sparking my interest in graphene and providing me with invaluable input and guidance for my research, all while coping with the difficulties of reduced contact due to the Corona pandemic. I also wish to thank Prof. Dr. Jan Carl Budich for kindly agreeing to take up the task to be the second reviewer of my project.

I thank my friends for their patience and understanding for my limited availability during the critical stage of my project. In particular, I would like to single out Tim Pokart for taking the time to provide me with incredibly useful peer-feedback in the final weeks.

I am endlessly grateful to my father for all the engaging and insightful discussions about physics and to the rest of my family for their endless tolerance thereof. Thank you for all your support and encouragement in my studies for the past three years and in the future.

I would like to give an honorable mention to the online support communities for Python, matplotlib, numpy and LaTeX as well as the Wikipedia organization, whose anonymous contributors greatly helped reduce my work load during my studies.

Finally, I gratefully acknowledge the HZDR for financially supporting this project.

Contents

1 Introduction

The discovery and examination of properties of novel materials is an important task of condensed matter physics and material science, motivated by the high industrial value of innovative technologies as well as the fundamendal knowledge that can be gained from studying the nature of matter. In 2004, the material graphene (consisting of a single two-dimensional layer of graphite) was first isolated and examined by Andre Geim and Konstantin Novoselov [1], an endeavor which earned them the Nobel Prize in Physics in 2010 [2].

Graphene has many unique properties making it the focus of ongoing research, especially for applications in semiconductor electronics. One particularly interesting property of graphene is that electrons behave as if they have no mass, meaning that we can consider them as ultrarelativistic[1] particles in the context of special relativity, similar to photons in a vacuum. Contrary to photons, electrons do also possess a non-zero electric charge and are therefore affected by electromagnetic fields. The fact that graphene effectively gives rise to massless charged particles, which are not known to exist as free states of the vacuum [3], motivates us to study the kinematics and dynamics of such particles in more detail.

In this work, we aim to examine and categorize semiclassical[2] trajectories of particles in graphene under the influence of specific stationary electromagnetic fields. We will begin in chapter 2 by reviewing the electronic properties of graphene as well as the formalism used to describe quantum particles in graphene. In chapter 3, we will restrict the problem to only certain electric and magnetic fields and then apply the WKB approximation method to obtain classical equations of motion. Additionally, we will examine the symmetries of the problem to improve our qualitative understanding of particle motion in graphene. Finally, we will present some methods of investigating the specific trajectories of particles for certain examples of electric fields in chapter 4.

---

[1] By *ultrarelativistic*, we refer to the property that particles are traveling at the maximum speed postulated by special relativity, which is only possible for particles with zero mass due to relativistic mass increase.

[2] In this context, *semiclassical* refers to a regime in which quantum effects can be neglected. We are however fully observing the law of special relativity.

2 Background

2.1 Electronic Properties of Graphene

A good overview of this topic is given in the textbook *The Physics of Graphene* by Mikhail Katsnelson [4] as well as the article *The electronic properties of Graphene* by Castro Neto et. al. [5]. This section is a brief summary of key information from these works.

Graphene is a two-dimensional material consisting of a single layer of carbon atoms arranged in a honeycomb lattice (triangular Bravais lattice with two atoms per elementary cell), as shown in Figure 2.1. The primitive lattice vectors are given by

$$\vec{a}_1 = \frac{a}{2}\left(3, \sqrt{3}\right), \qquad \vec{a}_2 = \frac{a}{2}\left(3, -\sqrt{3}\right), \tag{2.1}$$

where $a \approx 1.42\,\text{Å}$ is the distance between one carbon atom and its nearest neighbor.

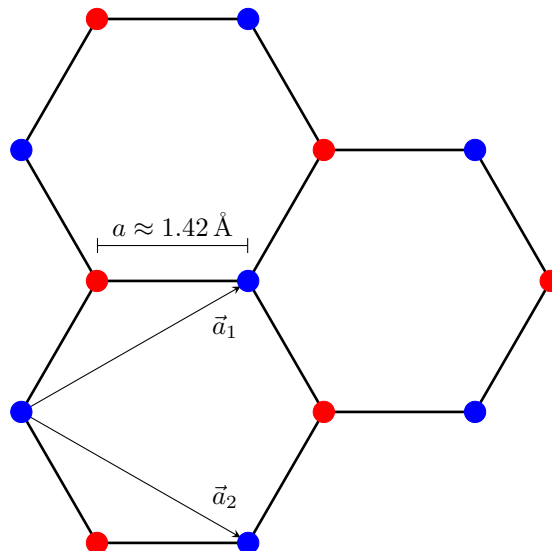**Figure 2.1:** Schematic of the graphene lattice consisting of two triangular sub-lattices (*red* and *blue*). The Bravais lattice is the blue triangular lattice defined by the primitive vectors $\vec{a}_1$ and $\vec{a}_2$. The nearest-neighbor distance of $a \approx 1.42\,\text{Å}$ is also shown.

The tight-binding model can be used to calculate the band structure of graphene. Considering only

nearest-neighbor interactions yields

$$E_{\pm}(\vec{k}) = \pm t\sqrt{3 + f(\vec{k})}, \tag{2.2}$$

where E_+ and E_- are the energies of the conduction and valence band, respectively, and

$$f(\vec{k}) = 2\cos(\sqrt{3}k_y a) + 4\cos\left(\frac{\sqrt{3}}{2}k_y a\right)\cos\left(\frac{3}{2}k_x a\right), \tag{2.3}$$

and where $t \approx 2.8\,\mathrm{eV}$ is the nearest-neighbor hopping energy. Interestingly, we notice that the two bands $E_{\pm}$ touch where $f(\vec{k}) = -3$, making graphene a zero bandgap semiconductor. These touching points are known as *Dirac points* and coincide with the corners of the first Brillouin zone. They are given by the vectors

$$\vec{K} = \frac{2\pi}{3a}\left(1, \frac{1}{\sqrt{3}}\right), \qquad \vec{K'} = \frac{2\pi}{3a}\left(1, -\frac{1}{\sqrt{3}}\right), \tag{2.4}$$

and translations thereof with a reciprocal lattice vector. If we expand (2.2) close to a Dirac point (for example $\vec{K}$) up to linear order in $\vec{q} := \vec{k} - \vec{K}$, we obtain

$$E_{\pm}(\vec{q}) \approx \pm v_F \hbar |\vec{q}|, \tag{2.5}$$

where $\vec{q}$ is the wave vector relative to the Dirac point and v_F is the Fermi velocity given by

$$v_F = \frac{3at}{2\hbar} \approx 10^6\,\mathrm{m/s}. \tag{2.6}$$

The linear dispersion relation obtained in (2.5) allows us to describe the electrons moving through graphene as ultrarelativistic particles within the context of special relativity. This means they effectively have no mass and move at the maximum speed allowed. We can use established relativistic theories but must make some modifications to describe the dynamics in this new paradigm. Most importantly, the electrons move through graphene at the Fermi-velocity v_F, which plays the role of the speed of light in our pseudorelativistic theory. It is important to note that it is not the fundamental characteristic of spacetime but the special structure of graphene that allows us to use an *analog* of special relativity as a description. The electrons move much too slowly (about 0.3% of the speed of light in a vaccuum) to give relevance to any true relativistic effects.

2.2 Dirac Formalism

2.2.1 Units and Notation

For simplicity's sake, we will now choose a natural system of units with $v_F = \hbar = q_e = 1$, where v_F is the Fermi velocity, $\hbar$ is the reduced Planck constant and q_e is the elementary charge.

We will also use index notation as is common in relativistic theories. The relativistic position vector is thereby defined by $x^\mu = (t, \vec{r})$. With respect to a Lorentz-transformation, contravariant quantities are indexed on top (e.g. x^μ) and covariant quantities are indexed at the bottom (e.g. x_μ). They are related via $x^\mu = g^{\mu\nu} x_\nu$, where $g^{\mu\nu}$ is the Minkowski-metric with signature $(+, -, -, -)$. Furthermore, we observe the Einstein summation convention by which there is an implied sum over indices that appear both at the top and at the bottom in a product (e.g. $x^\mu y_\mu = \sum_\mu x^\mu y_\mu$).

2.2.2 The Dirac Equation

The simplest way a relativistic quantum particle with a linear dispersion relation can be described is by a Lorentz-invariant equation that is linear in the energy operator $i\partial_t$ and the momentum operator $-i\nabla$. This equation is known as the free massless Dirac equation, first derived by Paul Dirac in a more general form in 1928 [6].

$$i\gamma^\mu \partial_\mu \Psi = 0 \tag{2.7}$$

A priori, γ^μ are just some coefficients letting the equation maintain its generality. Dirac's idea was to choose the γ^μ so that squaring the operator $i\gamma^\mu \partial_\mu$ reproduces the quantum analog of the massless energy-momentum relation $p^\mu p_\mu = E^2 - \vec{p}^2 = 0$, the free wave equation $\partial^\mu \partial_\mu \Psi = 0$. This translates into the following condition on γ^μ.

$$\gamma^\mu \gamma^\nu + \gamma^\nu \gamma^\mu = 2g^{\mu\nu} \tag{2.8}$$

In $(3 + 1)$-dimensional spacetime, γ^μ must be at least (4×4)-matrices in order to fulfill the above condition (and hence Ψ will be a wave function with 4 components). The specific choice of the set of γ–matrices is arbitrary. [7]

A description of planar graphene only requires two spatial dimensions. Therefore, we need only to find a set of three γ–matrices satisfying (2.8). This is possible using only (2×2)-matrices, for

example

$$\gamma^0 = \begin{pmatrix} 1 & 0 \\ 0 & -1 \end{pmatrix}, \qquad \gamma^1 = \begin{pmatrix} 0 & 1 \\ -1 & 0 \end{pmatrix}, \qquad \gamma^2 = \begin{pmatrix} 0 & -i \\ -i & 0 \end{pmatrix}, \tag{2.9}$$

We can introduce an external electromagnetic field by so-called minimal coupling, which transforms the energy-momentum operator as $i\partial_\mu \to i\partial_\mu - A_\mu$. This yields the following Dirac equation for a massless particle in an electromagnetic field.

$$i\gamma^\mu(\partial_\mu + iA_\mu)\Psi = 0 \tag{2.10}$$

This form of the Dirac equation with γ^μ as defined above will be basis of all further calculations. It is an accurate description of fermions in graphene when applying the continuum limit to the periodic lattice structure [5].

3 General Examinations

3.1 Semiclassical Treatment

3.1.1 Problem Specifications

The two axes of the Graphene sheet are labeled x and y. In this Thesis, we will consider stationary electromagnetic fields. The magnetic field $\vec{\mathcal{B}} = \mathcal{B}\vec{e}_z$ is homogeneous and perpendicular to the Graphene plane. The electric field[1] $\vec{\mathcal{E}}(x) = \mathcal{E}(x)\vec{e}_x$ is parallel to the x–axis but the spatial dependence of its magnitude will remain general at first and we will consider some interesting special cases in chapter 4. The pseudorelativistic potential A^μ can then be chosen as

$$A^\mu(x^\mu) = (\phi(x), 0, \mathcal{B}x), \tag{3.1}$$

where $\phi(x)$ is the electrostatic potential, related to the electric field by $\mathcal{E} = -\nabla\phi$. This is similar to the setup by Friedemann Queisser and Ralf Schützhold in [8], with the new addition of an electrostatic potential.

In the following part, we will use semiclassical approximations on the Dirac equation to obtain qualitative trajectories for the particles in graphene.

3.1.2 Decoupling the Dirac Equation

We must begin by further dissecting the Dirac equation for our specific problem. First, we notice that the electromagnetic potential is invariant under shifts in the t and y coordinates, prompting us to separate out a harmonic wave in these coordinates,

$$\Psi(t, x, y) = e^{-iEt+iky}\Psi^{E,k}(x). \tag{3.2}$$

---

[1] We are using the calligraphic $\mathcal{E}$ as a symbol for the electric field which is not to be confused with the energy later denoted by E.

Here, E and k are parameters corresponding to the energy of the particle and the y-component of its canonical momentum, respectively. The x-dependent part of the solution is now a two-component wave function $\Psi^{E,k} : \mathbb{R} \to \mathbb{C}^2$ for each pair (E, k).

Substituting the above separation ansatz as well as the electromagnetic potential (3.1) into (2.10) yields a matrix equation which can be read as a system of coupled differential equations for the two components the wave function $\Psi^{E,k} =: (\psi_1, \psi_2)$.

$$-i(\partial_x + k - \mathcal{B}x)\psi_2 = (E - \phi(x))\psi_1, \tag{3.3a}$$
$$-i(\partial_x - k + \mathcal{B}x)\psi_1 = (E - \phi(x))\psi_2. \tag{3.3b}$$

It is natural to try to decouple this system of equations into two separate equations for ψ_1 and ψ_2 by dividing by $(E - \phi(x))$ and substituting one equation into the other. Regarding the rules of differentiation with the ∂_x-operator, we obtain

$$\left[-\partial_x^2 + (k - \mathcal{B}x)^2 - \mathcal{B} + \frac{\phi'(x)(\partial_x - k + \mathcal{B}x)}{E - \phi(x)} \right] \psi_1 = (E - \phi(x))^2 \psi_1, \tag{3.4a}$$
$$\left[-\partial_x^2 + (k - \mathcal{B}x)^2 + \mathcal{B} - \frac{\phi'(x)(\partial_x + k - \mathcal{B}x)}{E - \phi(x)} \right] \psi_2 = (E - \phi(x))^2 \psi_2. \tag{3.4b}$$

However, we can see that these equations will be problematic for further analysis. They generally cannot be written in Schrödinger form as $E\psi_{1,2} = \left(\partial_x^2 + \mathcal{V}_{\text{eff}}(x) \right) \psi_{1,2}$, because the energy E is difficult to isolate. Furthermore, there are singular points at $E = \phi(x)$ that were artificially produced by the decoupling process.

3.1.3 Schrödinger Hamiltonian

An alternative possibility is to isolate E already in the original Dirac equation and interpret the remaining part of the equation as a Hamiltonian in matrix form. We begin by multiplying the Dirac equation with γ^0 from the left and expanding the sum.

$$\begin{aligned} \left(i\gamma^0\gamma^0\partial_t - \gamma^0\gamma^0\phi(x) + i\gamma^0\gamma^1\partial_x + i\gamma^0\gamma^2\partial_y + \gamma^0\gamma^2 Bx \right) \Psi = 0 \\ \Leftrightarrow i\partial_t\Psi = \left(-i\gamma^0\gamma^1\partial_x - i\gamma^0\gamma^2\partial_y + \phi(x) - \gamma^0\gamma^2\mathcal{B}x \right) \Psi \end{aligned} \tag{3.5}$$

Using the same separation ansatz (3.2), this yields

$$E\Psi^{E,k} = \left(-i\gamma^0\gamma^1\partial_x + \gamma^0\gamma^2(k - \mathcal{B}x) + \phi(x) \right) \Psi^{E,k} =: \mathcal{H}\Psi^{E,k}. \tag{3.6}$$

Now we have an equation that is form-equivalent to the Schrödinger equation, where the Hamiltonian $\mathcal{H}$ is the following hermitian matrix operator.

$$\mathcal{H} = \begin{pmatrix} \phi(x) & -i(\partial_x + k - \mathcal{B}x) \\ -i(\partial_x - k + \mathcal{B}x) & \phi(x) \end{pmatrix} \tag{3.7}$$

3.1.4 WKB Approximation

Continuing from the obtained Hamiltonian, we can apply the *Wenzel-Kramers-Brillouin* (WKB) approximation in order to find a semiclassical trajectory for the particle. The WKB approximation is a method for approximating solutions to linear differential equations with general coefficients. It is often applied to problems in quantum mechanics because with it one can easily derive the classical limit of the dynamics for scales where quantization is no longer relevant. The WKB approximation was first rigorously applied to the Dirac equation with a general electromagnetic field by Pauli [9]. We shall use a less formal approach than Pauli to tackle our specific problem by using a more intuitive interpretation of the WKB approximation.

We begin by writing the 2-component wave function using new functions $\Psi_0(x)$ and $S(x)$.

$$\Psi^{E,k}(x) = \Psi_0(x)e^{iS(x)}, \tag{3.8}$$

where

$$\Psi_0(x) =: \begin{pmatrix} \psi_1(x) \\ \psi_2(x) \end{pmatrix} \tag{3.9}$$

is a 2-component vector function representing the amplitude of the wave and $S(x)$ is a real function representing its phase. Formally, the WKB approximation consists in expanding $S(x)$ in orders of $\hbar$ with each individual term satisfying the Dirac equation up to that order. For the purpose of finding semiclassical trajectories (whose action is much larger than $\hbar$), considering only the zeroth order is sufficient and we can then identify $S'(x)$ as the x-component of the kinetic momentum p_x [10]. Furthermore, we assume that the amplitude $\Psi_0(x)$ varies slowly compared to the phase $S(x)$, yielding

$$\partial_x \Psi_j^{E,k} = \Big[\underbrace{iS'(x)}_{\text{Phase Variation}} + \underbrace{\frac{\varphi_j'(x)}{\varphi_j(x)}}_{\text{Amplitude Variation}} \Big] \Psi_j^{E,k} \approx iS'(x)\Psi_j^{E,k} = ip_x \Psi_j^{E,k} \tag{3.10}$$

for the x-derivative of each component of $\Psi^{E,k}$ ($j = 1, 2$). Substituting this and the ansatz (3.8) into

(3.6), we obtain the matrix equation

$$\begin{pmatrix} E - \phi(x) & -p_x + i(k - \mathcal{B}x) \\ -p_x - i(k - \mathcal{B}x) & E - \phi(x) \end{pmatrix} \Psi_0(x) = 0. \tag{3.11}$$

A condition for the existence of a solution $\Psi_0(x)$ is that the determinant of this matrix is zero for all x, which results in the energy-momentum relation

$$p_x^2 + (k - \mathcal{B}x)^2 = (E - \phi(x))^2. \tag{3.12}$$

This enables us to make progress towards analyzing semiclassical trajectories of particles. One more important point to note is we are only considering the classically allowed regions for particles, which are defined by the condition $p_x \in \mathbb{R}$. Additionally, we will first only consider trajectories with non negative kinetic energy, i.e. $E \geq \phi(x)$. However, we will later see that solutions with $E < \phi(x)$ do have some interpretational value, namely as so-called "antiparticles" in Dirac theory or "holes" in the context of graphene.

3.2 Equations of Motion

3.2.1 Classical Hamilton Formalism

Before we derive the equations of motion governing the particle in graphene, it is useful to summarize the classical Hamiltonian mechanics describing ultrarelativistic motion. Our starting point is the Hamiltonian function describing the total energy of a particle in an electromagnetic potential, which consists of the particle's kinetic energy and its electrostatic potential energy.

$$\mathcal{H}(\vec{x}, \vec{p}) = \vec{p} \cdot \vec{v} + \phi(\vec{x}) \tag{3.13}$$

In this equation $\vec{p}$ describes the kinetic momentum of the particle. However, in order for the formalism to yield the correct results, we must choose the canonical momentum as $\vec{P} = \vec{p} + \vec{A}(\vec{x})$:

$$\mathcal{H}(\vec{x}, \vec{P}) = \left(\vec{P} - \vec{A}(\vec{x})\right) \cdot \vec{v} + \phi(\vec{x}) \tag{3.14}$$

Then, the Hamilton-Jacobi equations give us time evolution of the canonical momentum.

$$\dot{\vec{P}} = -\nabla \mathcal{H} = \nabla(\vec{A}(\vec{x}) \cdot \vec{v}) - \nabla \phi(\vec{x}) \tag{3.15}$$

For the time evolution of the kinetic momentum, it follows

$$
\begin{aligned}
\dot{\vec{p}} &= \dot{\vec{P}} - \frac{\mathrm{d}\vec{A}(\vec{x})}{\mathrm{d}t} \\
&= \dot{\vec{P}} - (\vec{v} \cdot \nabla)\vec{A}(\vec{x}) \\
&= \nabla(\vec{A}(\vec{x}) \cdot \vec{v}) - (\vec{v} \cdot \nabla)\vec{A}(\vec{x}) - \nabla\phi(\vec{x}) \\
&= \vec{v} \times (\nabla \times \vec{A}(\vec{x})) - \nabla\phi(\vec{x}) \\
&= \vec{v} \times \vec{\mathcal{B}} + \vec{\mathcal{E}}.
\end{aligned}
\tag{3.16}
$$

This is the Lorentz force, as expected.

We have now gained some useful insight regarding the difference between kinetic and canonical momentum. Within a quantized theory, the momentum operator $-i\nabla$ corresponds to the classical *canonical* momentum. Relating this back to our specific setup, this means that the x-components of the canonical and kinetic momenta are equal, since $A_x = 0$. The y-component of the canonical momentum has been separated out in (3.2) and is now described by the eigenvalue k. This means that the kinetic momentum in y-direction is given by

$$
p_y = k - \mathcal{B}x.
\tag{3.17}
$$

With this, the semiclassical energy-momentum relation (3.12) rearranges to

$$
p_x^2 + p_y^2 = (E - \phi(x))^2,
\tag{3.18}
$$

which allows us to define the total momentum p as

$$
p := |\vec{p}| = \sqrt{p_x^2 + p_y^2} = E - \phi(x),
\tag{3.19}
$$

under the condition $E \geq \phi(x)$. Rearranging this, we obtain

$$
E = |\vec{p}| + \phi(x),
\tag{3.20}
$$

which – considering that in the chosen system of units, the velocity is a unit vector parallel to $\vec{p}$ – corresponds exactly to the classical Hamiltonian function (3.13).

3.2.2 Effective Potential and Behavior at the Turning Points

If we are interested in the qualitative motion along the x-axis, we can rearrange the energy-momentum relation (3.12) into a form with an effective potential.

$$p_x^2 + \mathcal{V}_{\text{eff}}(x) = 0 \qquad \text{with} \qquad \mathcal{V}_{\text{eff}}(x) = (k - \mathcal{B}x)^2 - (E - \phi(x))^2 \tag{3.21}$$

If we take the time derivative of this equation, we obtain

$$2p_x \dot{p}_x + \mathcal{V}'_{\text{eff}}(x)\dot{x} = 0. \tag{3.22}$$

Since $\dot{\vec{x}}$ is parallel to $\vec{p}$ and has unit magnitude, we see that $\dot{x} = \frac{p_x}{p}$, which gives us

$$\dot{p}_x = -\frac{1}{2p(x)}\mathcal{V}'_{\text{eff}}(x) = \frac{\mathcal{B}(k - \mathcal{B}x)}{E - \phi(x)} - \phi'(x). \tag{3.23}$$

Since $p(x) = E - \phi(x)$ is by choice non-negative for all x, we can recognize the direction of an effective force in x-direction by the negative gradient of the effective potential $\mathcal{V}_{\text{eff}}$. The classical turning points on the x-axis are the roots of $\mathcal{V}_{\text{eff}}(x)$. We note that these are generally distinct from the turning points in the electrostatic potential by itself ($E = \phi(x)$), since the magnetic field will tend to cause a particle to curve away from those before reaching them.

However, we will later see that specific initial conditions can theoretically make a particle reach $E = \phi(x)$, so it is worth giving this case some attention. The situation $E = \phi(x)$ means that the total momentum vanishes. In particular, $p_x = 0$ and $p_y = k - \mathcal{B}x = 0$. As $\mathcal{V}_{\text{eff}} = 0$ at this point, it is a turning point of the trajectory. In (3.23), we can then use L'Hôpital's rule to evaluate the fraction in the limit of x approaching the turning point, as both the numerator and denominator tend to zero in this limit. With this, we obtain

$$\dot{p}_x = \frac{\mathcal{B}^2}{\phi'(x)} - \phi'(x), \qquad \text{for } E = \phi(x). \tag{3.24}$$

This equation is not valid if the electric field vanishes at the turning point. In this case, the particle would just stay stationary at the turning point since it has no force acting on it. It is also worth discussing the possibility that $\dot{p}_x$ has a different sign than $-\phi'(x)$, since that would then accelerate the particle outside the classically allowed region. This is the case if and only if

$$\mathcal{B}^2 > \phi'(x)^2, \tag{3.25}$$

i.e. the electric field is *subcritical* at the turning point. When we consider the specific trajectories for a homogeneous electric field in section 4.2, we will see that $E = \phi(x)$ can never be reached for this case. If the electric field is *supercritical*, i.e. $\mathcal{B}^2 < \phi'(x)^2$, the potential barrier at $E = \phi(x)$

can indeed be reached and the particle will undergo a hard reflection, meaning its velocity will discontinuously reflect on the y-axis when p_x switches sign.

3.2.3 Equations of Motion

In order to calculate full two-dimensional trajectories, we also need an equation for the time evolution of the y-momentum, which is given by

$$\dot{p}_y = \frac{\mathrm{d}}{\mathrm{d}t}(k - \mathcal{B}x) = -\mathcal{B}\dot{x}. \tag{3.26}$$

Since we wish to produce visualizations of the trajectories in later chapters, we need equations directly describing the acceleration of the particle as a function of its velocity and position, which we can then integrate numerically. In an ultrarelativistic setting, the relation between the force and the acceleration is not as simple as Newton's second law. It can be calculated as follows.

$$\ddot{x} = \frac{\mathrm{d}}{\mathrm{d}t}\dot{x} = \frac{\mathrm{d}}{\mathrm{d}t}\left(\frac{p_x}{p}\right) = \frac{\dot{p}_x p - p_x \dot{p}}{p^2} \qquad \text{(and analogous for } \ddot{y}) \tag{3.27}$$

With $p = E - \phi(x)$, we obtain

$$\dot{p} = -\phi'(x)\dot{x}. \tag{3.28}$$

Substituting (3.23), (3.26), (3.28) into (3.27) yields the desired equations.

$$\ddot{x} = \dot{y}\frac{\mathcal{B}}{E - \phi(x)} - \dot{y}^2\frac{\phi'(x)}{E - \phi(x)}, \tag{3.29a}$$

$$\ddot{y} = -\dot{x}\frac{\mathcal{B}}{E - \phi(x)} + \dot{x}\dot{y}\frac{\phi'(x)}{E - \phi(x)} \tag{3.29b}$$

This system of equations describes the ultrarelativistic motion of charged particles in the given electromagnetic field. They are non-linear and are generally difficult to solve analytically except for some specific potentials. As usual for a system of two second-degree differential equations, there are four degrees of freedom specified by four initial conditions. Two of them can be chosen as the initial position. The initial velocity cannot be completely freely chosen, as its magnitude is fixed at 1. It therefore only takes one degree of freedom specifying its initial direction. The fourth degree of freedom is the energy E.

3.3 Symmetries

Before going on to analyze specific trajectories, we can benefit from considering the behavior of the physical system when undergoing certain natural transformations. This will enable us to discover certain symmetries in the problem, which will deepen our understanding of the underlying physics and also save time when categorizing trajectories qualitatively. We consider the Schrödinger form of the Dirac equation given by (3.6).

$$
\begin{pmatrix} \phi(x) & -i(\partial_x + k - \mathcal{B}x) \\ -i(\partial_x - k + \mathcal{B}x) & \phi(x) \end{pmatrix} \Psi^{E,k} = E\Psi^{E,k}
\tag{3.30}
$$

3.3.1 Negative Energies, Time Reversal and Charge Conjugation

In deriving the semiclassical equations of motion, we have on multiple instances assumed that the particle possesses non-negative kinetic energy, i.e. $E \geq \phi(x)$ at all points on its trajectory. This may seem like a reasonable assumption from the point of view of classical mechanics, but it is in fact not at all a requirement of the Dirac equation. Given that $\Psi^{E,k}$ is a solution of (3.30), we can easily verify that $\sigma^z\Psi^{E,k}$ is then a solution[2] of the equation where the signs of E and ϕ have been reversed.

Now we are faced with the question of how to interpret these negative energy solutions within the context of classical motion. We notice that switching the sign of E is equivalent to time-reversal of the wave function because of $\Psi \sim e^{-iEt}$. Instead of reversing the time of the wave function, we can also just reverse the time of the external fields to get the same qualitative laws of motion. The transformational behavior of the electric and magnetic fields was examined in simple terms by Kaplan and Tsankov [11]: time reversal leaves the electric field invariant but reverses the magnetic field. Thus, we find that a solution of the Dirac equation with E and $\phi(x)$ reversed is qualitatively equivalent to a solution with B and $\phi(x)$ reversed, which is effectively achieved by charge conjugated particle in the same external field.

This means that we can interpret the negative energy solutions as particles with the opposite charge. In Dirac's original theory, this thought experiment led to the postulation of an oppositely charged counterpart of the electron later known as the positron[3] [12]. To prevent electrons from perpetually falling into lower energy states, all negative energy states were assumed to be already occupied by electrons, a model known as the "Dirac sea". A positron is then interpreted as a hole in the Dirac sea, implying that a positron-electron pair may be created by using energy to elevate an electron

---

[2]Where $\sigma^z = \begin{pmatrix} 1 & 0 \\ 0 & -1 \end{pmatrix}$ is the third Pauli matrix.

[3]In his 1930 paper, Dirac incorrectly inferred that the proton, not the positron, was the antiparticle to the electron. This was refuted soon after the publication and the positron was experimentally confirmed two years later in 1932.

out of the sea. This model raises certain issues when used to describe the vaccuum, such as the supposedly infinite mass and charge density of the Dirac sea. However, in the context of condensed matter physics, the substrate on which the electrons move is made of matter, in which we do indeed observe holes (missing electrons) behave as positively charged quasiparticles.

3.3.2 Parity Transformations

A *parity transformation* or *parity reversal* is usually defined as the inversion of the position vector $\vec{r}$, which turns a right-handed basis into a left-handed one in three-dimensional space. However, in the present two-dimensional system, the inversion of the position vector is simply a rotation by $180°$ around the origin. Since we wish to examine reflections, we will define the parity reversal as being the inversion of only *one* spatial coordinate, either x or y.

First, we examine the Dirac equation if we mirror the system on the x-axis, i.e. $y \to -y$. This is equivalent to reversing the sign of k because of $\Psi \sim e^{iky}$. If we reverse k in (3.30), we can see that we can retain symmetry if we also reverse the magnetic field $\mathcal{B}$: If $\Psi^{E,k}$ is a solution of the original Dirac equation (3.30), then $\sigma^x \Psi^{E,k}$ is a solution[4] of the equation where k as well as $\mathcal{B}$ have been reversed. We can show that $\Psi^{E,k}$ and $\sigma^x \Psi^{E,k}$ qualitatively describe the same trajectory. Starting from

$$\mathcal{H}\Psi^{E,k} = E\Psi^{E,k}, \tag{3.31}$$

we multiply with σ^x from the left and insert $\sigma^x \sigma^x = \mathbf{1}$.

$$\underbrace{\sigma^x \mathcal{H} \sigma^x}_{=:\mathcal{H}'} \sigma^x \Psi^{E,k} = E \sigma^x \Psi^{E,k} \tag{3.32}$$

When applying the WKB approximation, we saw that the energy-momentum relation only depends on the determinant of $\mathcal{H} - E$ (where ∂_x has been replaced with ip_x), which can easily be shown to be equal to the determinant of $\mathcal{H}' - E$.

$$\begin{aligned}
\det(\mathcal{H}' - E) &= \det(\sigma^x \mathcal{H} \sigma^x - E) = \det(\sigma^x \mathcal{H} \sigma^x - \sigma^x E \sigma^x) \\
&= \det(\sigma^x (\mathcal{H} - E)\sigma^x) = \det(\sigma^x)\det(\mathcal{H} - E)\det(\sigma^x) = \det(\mathcal{H} - E)
\end{aligned} \tag{3.33}$$

Of course, this also works if we choose any other matrix M with the property $M^2 = 1$ instead of σ^x.

In summary, this means that if a trajectory satisfies the semiclassically approximated Dirac equation,

---

[4]Where $\sigma^x = \begin{pmatrix} 0 & 1 \\ 1 & 0 \end{pmatrix}$ is the first Pauli matrix.

its reflection on the x-axis will do so for a reversed $\mathcal{B}$. This allows us to limit ourselves to $\mathcal{B} \geq 0$ in chapter 4 without loss of generality.

Now, we consider mirroring the system on the y-axis, i.e. $x \to -x$. Since the electrostatic potential depends on x, we cannot give a general answer to the question of what this parity transformation does, so we will limit ourselves to electrostatic potentials possessing some symmetry in x. Specifically, we have two cases:

- The potential is symmetric. $\Longleftrightarrow \phi(-x) = \phi(x)$

  Noting that the reversal of the x-coordinate in the Hamiltonian of (3.30) also reverses the derivative ∂_x, we find that we can retain the invariance of the equation by also reversing the magnetic field $\mathcal{B}$: If $\Psi^{E,k}$ is a solution of the original Dirac equation, then $\sigma^y \Psi^{E,k}$ is a solution[5] to the Dirac equation where x and $\mathcal{B}$ have been reversed. In analogy to the explanation given on the previous page, these two solutions qualitatively describe the same trajectories. Therefore, the reversal of $\mathcal{B}$ is qualitatively equivalent to the reversal of x, provided that the electrostatic potential is symmetric.

- The potential is antisymmetric. $\Longleftrightarrow \phi(-x) = -\phi(x)$

  Proceeding in analogy to the first case, we find that we can retain the qualitative invariance of the Hamiltonian by also reversing the electric potential ϕ *as well as* the magnetic field B.

Combining these two cases with our knowledge of the parity reversal in y, we can already make an interesting observation. For antisymmetric potentials, we find that flipping only the electric field corresponds to a reversal of both x- and y-coordinates, i.e. there is no qualitative difference in the motion other than point reflection on the origin. We can exploit this symmetry to limit our choice of parameters for the examples in chapter 4, again without loss of generality. However, for symmetric potentials, there is no simple geometric transformation that corresponds to the reversal of the electric field. This means that reversing the electric field can result in qualitatively different solutions, for example turning bound trajectories into unbound ones.

---

[5]Where $\sigma^y = \begin{pmatrix} 0 & -i \\ i & 0 \end{pmatrix}$ is the second Pauli matrix.

4 Specific Example Cases

4.1 Pure Magnetic Field

We begin by examining the simplest possibility, the case without an electric field. This means that $\phi(x)$ is a constant that we can choose as zero. For this case, the equations of motion (3.29) reduce to the following linear system of differential equations.

$$\ddot{x} = \dot{y}\frac{\mathcal{B}}{E},\tag{4.1a}$$

$$\ddot{y} = -\dot{x}\frac{\mathcal{B}}{E}\tag{4.1b}$$

Because of symmetry arguments, we can assume $\mathcal{B} > 0$. The above equations can then be analytically solved by clockwise circular motion with angular velocity ω given by

$$\omega = \frac{\mathcal{B}}{E}.\tag{4.2}$$

Since the particle always travels at unit velocity, $\omega R_0 = 1$ yields the radius R_0 of the circle.

$$R_0 = \frac{E}{\mathcal{B}}\tag{4.3}$$

Interestingly, we reproduce the Landau quantization in monolayer graphene as calculated by Yin et. al. [13] by (re-)quantizing this trajectory by using the Wilson-Sommerfeld [14, 15] rule. We parametrize the x-component of the orbit with $x = R_0 \cos\varphi$ and $p_x = -p\sin\varphi$, and note $p = E - \phi(x) = E$, which yields

$$\oint p_x \, \mathrm{d}x = \int_0^{2\pi} pR_0 \sin^2\varphi \, \mathrm{d}\varphi = \pi pR_0 = \pi\frac{E^2}{\mathcal{B}} \stackrel{!}{=} 2\pi n, \qquad (n = 1, 2, \ldots)$$

$$\implies E = \pm\sqrt{2n\mathcal{B}}.\tag{4.4}$$

4.2 Homogeneous Electric Field

Now we introduce a homogenous electric field with field strength $\mathcal{E}$ towards positive x in addition to the homogeneous magnetic field $\mathcal{B}$. The electrostatic potential is then given by

$$\phi(x) = -\mathcal{E}x. \tag{4.5}$$

Symmetry arguments allow us to choose $\mathcal{B} \geq 0$ and $\mathcal{E} \geq 0$ without loss of generality (See subsection 3.3.2 on parity transformations). For clarity, we will define the dimensionless parameter β relating the electric and magnetic fields as follows.

$$\beta := \frac{\mathcal{E}}{\mathcal{B}} \geq 0 \tag{4.6}$$

If the electric field is small, we can expect the trajectory to be bounded in x-direction by the magnetic field, the extreme case of this being the circular trajectory for a vanishing electric field. However, if the electric field is large enough, the particle can escape to $x \to \infty$. We will now consider these cases more precisely, starting with the unbounded case.

4.2.1 Unbounded Trajectory

A simple unbounded trajectory is a straight line with a non-zero x-component. We can examine under what conditions such a trajectory is a solution of the equations of motion (3.29). For this, we introduce the coordinate α defining the angle of velocity.

$$\begin{aligned} \dot{x} &= \cos \alpha, \\ \dot{y} &= \sin \alpha \end{aligned} \tag{4.7}$$

Linear motion is equivalent to the simple condition $\dot{\alpha} = 0$. Substituting (4.7) as well as

$$\begin{aligned} \ddot{x} &= -\dot{\alpha} \sin \alpha, \\ \ddot{y} &= \dot{\alpha} \cos \alpha \end{aligned} \tag{4.8}$$

into the equations of motion (3.29) yields a single differential equation for α.

$$\dot{\alpha} = -\frac{\mathcal{B}}{E + \mathcal{E}x} \left(1 + \beta \sin \alpha\right) \tag{4.9}$$

A stationary solution for α exists if and only if $\beta \geq 1$, i.e. $\mathcal{E} \geq B$. In this case we call the electric field *critical* ($\mathcal{E} = B$) or *supercritical* ($\mathcal{E} > \mathcal{B}$). Let us first consider the case $\mathcal{E} > \mathcal{B}$. Then there are

exactly two angles α_+ and α_- which satify the condition for linear motion.

$$\alpha_+ = -\arcsin\left(\frac{1}{\beta}\right), \qquad \alpha_- = \pi + \arcsin\left(\frac{1}{\beta}\right) \tag{4.10}$$

The angle $\alpha_+ \in \left(-\frac{\pi}{2}, \frac{\pi}{2}\right)$ defines a motion towards positive x, whereas $\alpha_- \in \left(\frac{\pi}{2}, \frac{3\pi}{2}\right)$ defines a motion towards negative x. These two solutions are the only fixed points of the time evolution of α. We can show that any other initial condition for α will converge toward α_+ for $t \to \infty$, i.e. α_+ is a stable and α_- an unstable fixed point. For this, we expand (4.9) around the fixed points $\alpha_\pm$ up to the linear term.

$$\dot{\alpha} = -\frac{\mathcal{E}}{E + \mathcal{E}x}\cos(\alpha_\pm)(\alpha - \alpha_\pm) + \mathcal{O}\left((\alpha - \alpha_\pm)^2\right) \tag{4.11}$$

Since $\cos\alpha_+ > 0$ and $\cos\alpha_- < 0$, α is attracted to α_+ and repulsed from α_-.

If we consider the limiting case $\beta = 1$, we obtain only one fixed point at $\alpha_0 = -\frac{\pi}{2}$ (motion parallel to the y-axis). Since $\cos\alpha_0$ vanishes, we must consider the quadratic order of (4.9) near the fixed point.

$$\dot{\alpha} = -\frac{\mathcal{E}}{2(E + \mathcal{E}x)}(\alpha - \alpha_0)^2 + \mathcal{O}\left((\alpha - \alpha_0)^3\right) \tag{4.12}$$

We see that this corresponds to a semi-stable fixed point, meaning it is attractive on one side and repulsive on the other. Because of the periodic nature of α, initial angles on the repulsive side will simply wrap around and approach it from its attractive side.

We must still examine the physical validity of the left-bound solution α_-.[1] Since this particle is traveling against the electric field, it would eventually reach the potential barrier at $x = -\frac{E}{\mathcal{E}}$, at which point (4.9) breaks down. In this case it is helpful to reconsider the time evolution of the x-momentum set forth in (3.24) specifically for this case. At the potential barrier, we have

$$\dot{p}_x = -\frac{\mathcal{B}^2}{\mathcal{E}} + \mathcal{E}. \tag{4.13}$$

For $\beta > 1$, $\dot{p}_x$ is positive, meaning the particle will indeed be accelerated back into the classically allowed region. Since the momentum vector $\vec{p} = (\pm\sqrt{(E - \phi(x))^2 - p_y^2}, k - \mathcal{B}x)^\top$ is purely a function of x except for the arbitrary sign of p_x, the particle will travel back in positive x direction with the same momentum that has been reflected in its x-component. This change is continuous for the momentum, since it vanishes at the turning point, but discontinuous for the velocity since its magnitude is fixed and only the direction changes. Thus, the left-bound trajectory is reflected on the

---

[1]Since this solution only exists for a singular initial condition, it practically cannot be realized. However, it is still a theoretical possibility, so we investigate it further.

potential barrier according to the law of reflection, which results in the stable right-bound trajectory, since α_+ and α_- are reflections of each other.

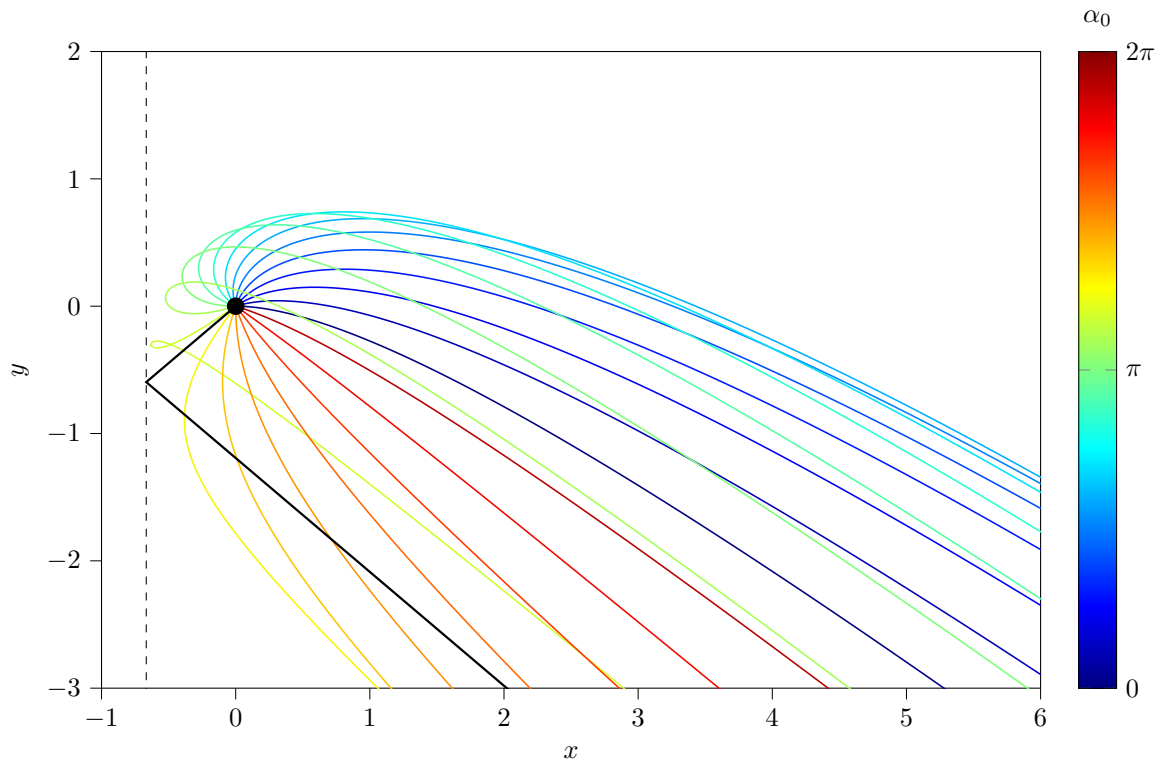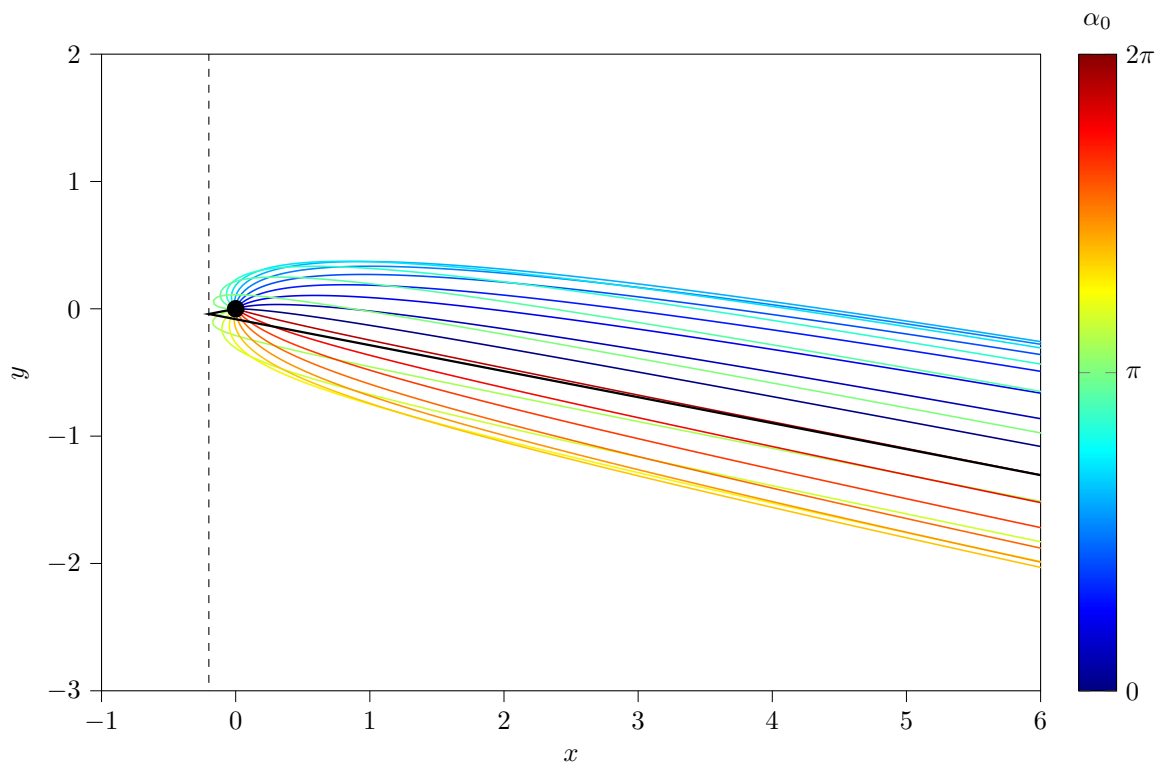Examples of unbounded trajectories are shown in Figure 4.1.

(a) $\beta = 1.5$

(b) $\beta = 5$

Figure 4.1: Examples of unbounded trajectories for two different β and various initial angles α_0. The starting point is the origin, shown as a black dot. Here, we have chosen $E = 1$ and $\mathcal{B} = 1$, making the axes dimensionless. Both plots have the same scaling. The potential barrier is shown as a black dashed line at $x = -\frac{1}{\beta}$. The thicker black line shows the trajectory starting at $\alpha_0 = \alpha_-$, leading to hard reflection. We see that other starting angles curve away from this trajectory.

4.2.2 Bounded Trajectory

Now let us consider the case $\beta < 1$, i.e. $\mathcal{E} < \mathcal{B}$. In this case, the electric field is called *subcritical* and we can transform it away by a Lorentz boost in y-direction. The equations of motion – having been derived from the Lorentz invariant Dirac equation – are also invariant under Lorentz boost, meaning that the choice of reference frame is arbitrary and this operation is justified. Specifically, with the pseudorelativistic potential $A^\mu = (-\beta\mathcal{B}x, 0, \mathcal{B}x)$, Lorentz matrix Λ, boost velocity v and Lorentz factor $\gamma = (1 - v^2)^{-\frac{1}{2}}$, the Lorentz boosted potential $A^{\mu\prime}$ is given by

$$A^{\mu\prime} = \Lambda^\mu{}_\nu A^\nu = \begin{pmatrix} \gamma & 0 & -v\gamma \\ 0 & 1 & 0 \\ -v\gamma & 0 & \gamma \end{pmatrix} \begin{pmatrix} -\beta\mathcal{B}x \\ 0 \\ \mathcal{B}x \end{pmatrix} = \begin{pmatrix} -\gamma\mathcal{B}(\beta+v)x \\ 0 \\ \gamma\mathcal{B}(v\beta+1)x \end{pmatrix} \stackrel{!}{=} \begin{pmatrix} 0 \\ 0 \\ \mathcal{B}'x' \end{pmatrix}. \qquad (4.14)$$

We find that the electric field disappears in the moving frame of reference if we choose $v = -\beta$, which is possible if and only if $\beta < 1$. Noting that $x' = x$ since the boost is perpendicular to x, we obtain the magnetic field in the moving frame by substituting $\beta = -v$ into the third component of the last equation, yielding

$$\mathcal{B}' = \gamma(1 - v^2)\mathcal{B} = \frac{\mathcal{B}}{\gamma}. \qquad (4.15)$$

In the transformed system, we already know that the solution to the equations of motion is a circular trajectory with radius R given by

$$R = \frac{E'}{\mathcal{B}'} = \gamma\frac{E'}{\mathcal{B}} \qquad (4.16)$$

In the laboratory system, R is the radius of the oscillation in x-direction. The energy in the transformed system is obtained with a Lorentz transformation on the relativistic momentum $p^\mu = (E - \phi(x), p_x, p_y) = (E + \beta\mathcal{B}x, p_x, k - \mathcal{B}x)$.

$$E' = \gamma(E + \beta\mathcal{B}x) + \beta\gamma(k - \mathcal{B}x) = \gamma(E + \beta k) \qquad (4.17)$$

The parameter k is not easy to interpret in the context of classical motion since it does not represent any obvious physical quantity. However, we can express it in terms of more intuitive initial conditions. Since we have homogeneous fields, we can freely choose the particle to start at the origin, i.e. $x_0 = y_0 = 0$. Let α_0 be the initial angle of motion. Then the initial y-momentum can be calculated in two ways.

$$p_y|_{t=0} = k - \mathcal{B}x_0 = k, \qquad (4.18a)$$

$$p_y|_{t=0} = p\sin\alpha_0 = (E + \mathcal{E}x_0)\sin\alpha_0 = E\sin\alpha_0 \qquad (4.18b)$$

Equating these two equations, we obtain

$$k = E \sin \alpha_0. \tag{4.19}$$

Inserting this into (4.17) yields

$$E' = \gamma E(1 + \beta \sin \alpha_0). \tag{4.20}$$

Finally, we obtain the radius of the oscillation with (4.16), noting $\gamma^{-2} = 1 - v^2 = 1 - \beta^2$.

$$R = R_0 \frac{1 + \beta \sin \alpha_0}{1 - \beta^2}, \tag{4.21}$$

where $R_0 = \frac{E}{\mathcal{B}}$ is the radius of the motion with no electric field. This relationship is shown in Figure 4.2. The period T' of one orbit in the moving reference frame is simply its length $2\pi R$. Because of time dilation, the period of the oscillation in the laboratory system is given by

$$T = \frac{T'}{\gamma} = 2\pi R_0 \frac{1 + \beta \sin \alpha_0}{\sqrt{1 - \beta^2}}. \tag{4.22}$$

Now is the time to revisit a statement made in subsection 3.2.2, claiming that in a subcritical electric field, the particle may never reach the potential barrier at $x_B = -\frac{E}{\mathcal{E}}$. Since there is no potential barrier for $\mathcal{E} = 0$, let $\beta > 0$. We can now prove that $x > x_B$ at all points on the trajectory. The lower bound of x (left turning point) $x_{\min}$ of the trajectory can be expressed as a function of β and α_0 by a more lengthy calculation we have left to Appendix A.1, resulting in

$$x_{\min} = R_0 \frac{(\sin \alpha_0 - 1)}{1 + \beta}. \tag{4.23}$$

This relationship is illustrated in Figure 4.3, by which we recognize that for any given β, the lowest possible $x_{\min}$ is reached by launching the particle towards negative y (i.e. $\alpha_0 = -\frac{\pi}{2}$) and is still strictly greater than x_B (for analytical proof also see Appendix A.1).

Thus, a particle will never reach the potential barrier for subcritical electric fields. Intuitively, this can be explained by the magnetic field making the particle curve away from the barrier. The more the particle loses momentum approaching the barrier, the stronger the curvature. Of course we can generalize this statement to include inhomogeneous (continuous) fields, since we need only consider the behavior of the particle in proximity of the barrier, where we can locally approximate the electric field as a constant.
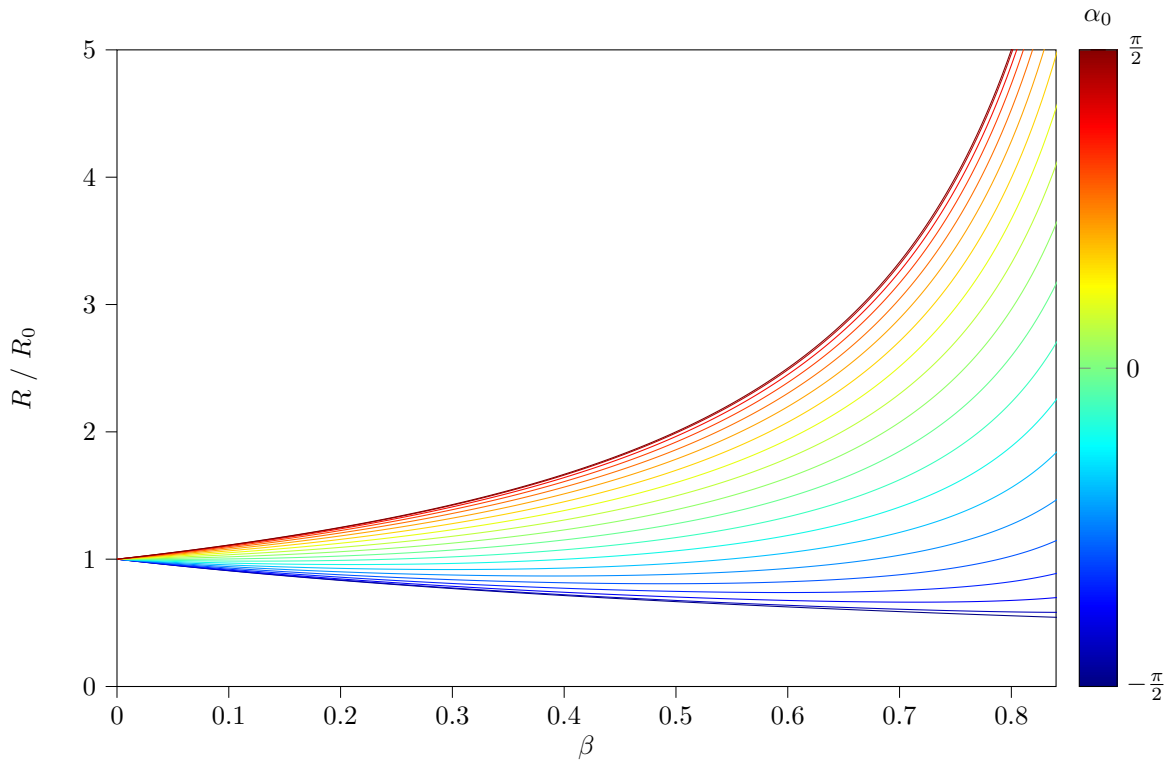
Examples of bounded trajectories are shown in Figure 4.4.

Figure 4.2: Radius R of the x-oscillation as a function of β for different initial angles α_0. The y-axis is in units of R_0.
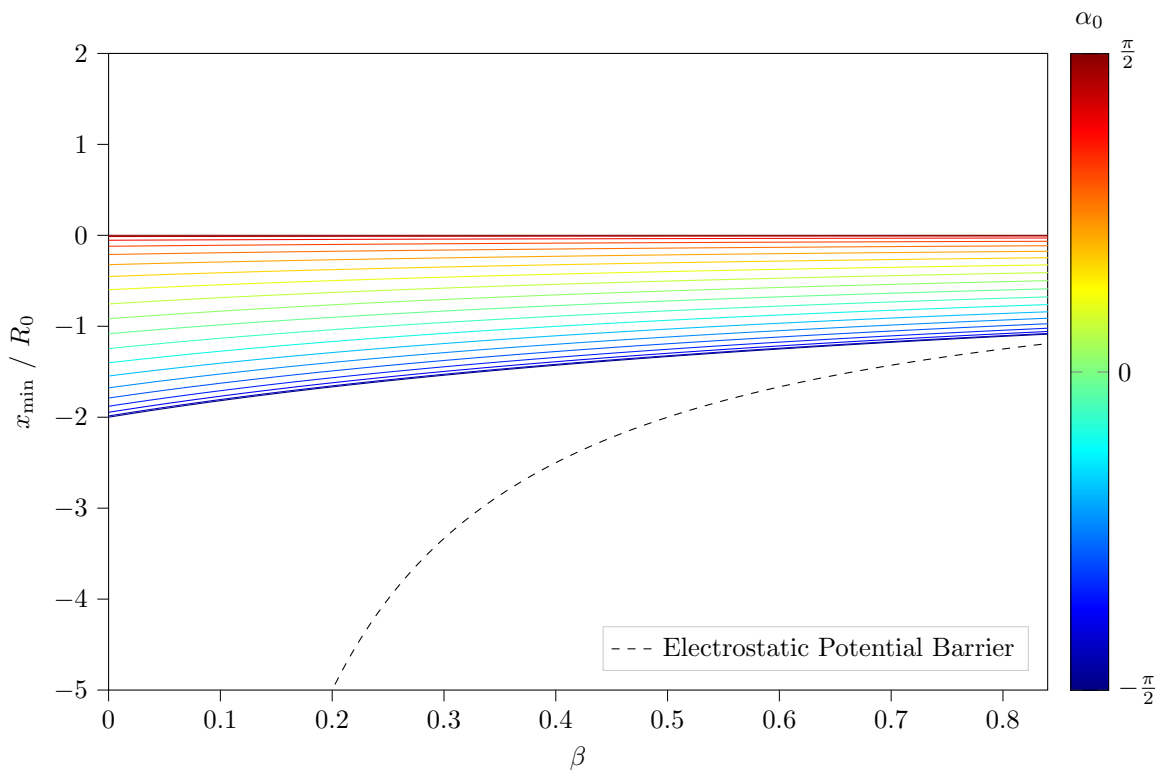

Figure 4.3: Left turning point $x_{\min}$ of the x-oscillation as a function of β for different initial angles α_0. The y-axis is in units of R_0. The electrostatic potential barrier at $x_B = -\frac{R_0}{\beta}$ is also shown.
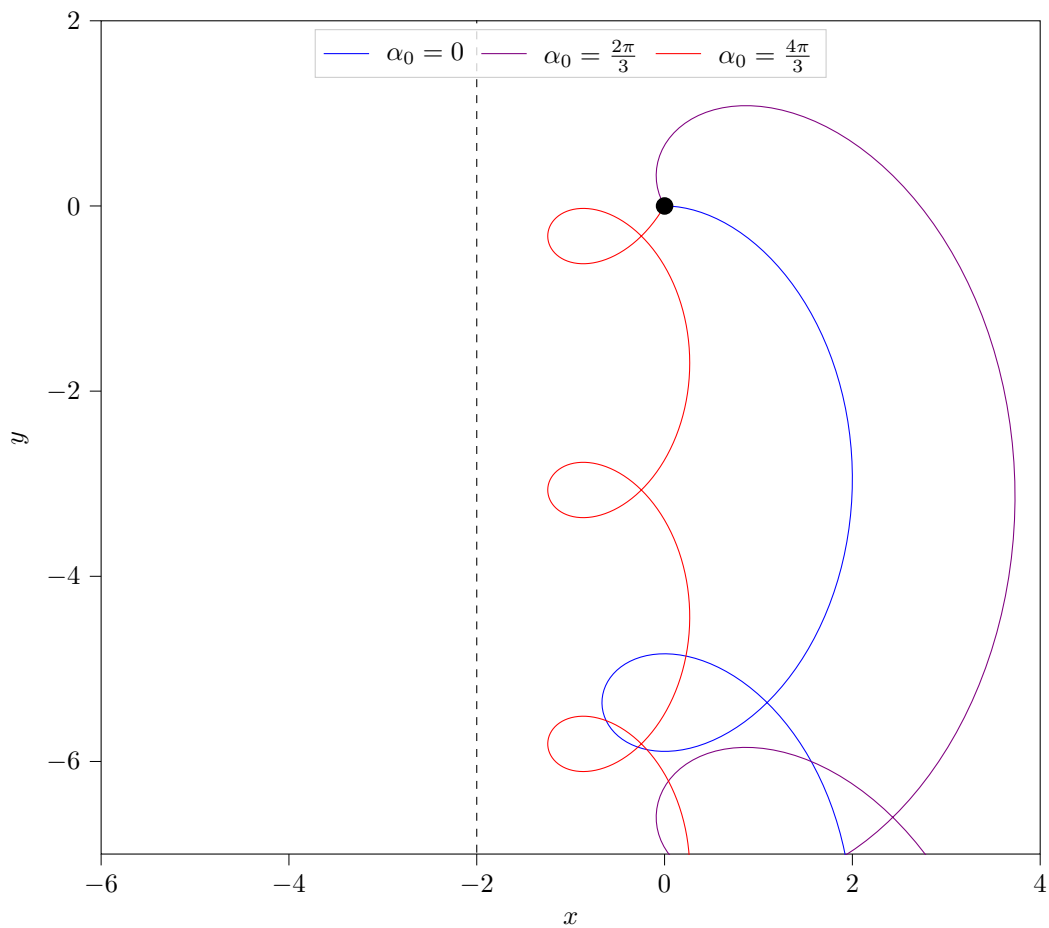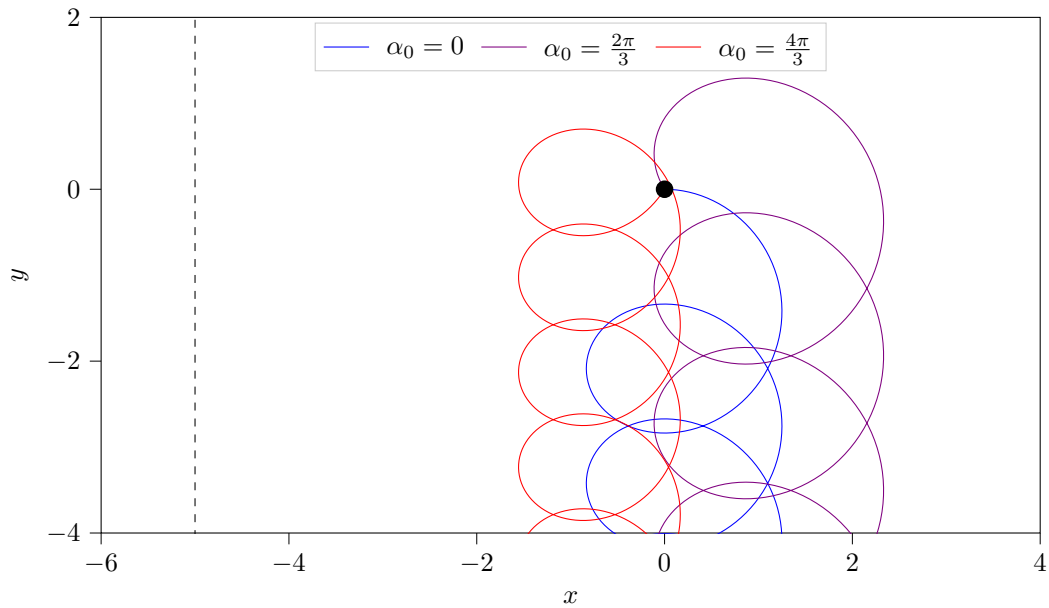
(a) $\beta = 0.2$

(b) $\beta = 0.5$

Figure 4.4: Examples of bounded trajectories for two different β and three initial angles α_0. The starting point is the origin, shown as a black dot. Here, we have chosen $E = 1$ and $\mathcal{B} = 1$, making the axes dimensionless. Both plots have the same scaling. The potential barrier is shown as a black dashed line at $x_B = -\frac{1}{\beta}$.

4.2.3 Drift Velocity

We can quantify the macroscopic motion of a particle in homogeneous fields by defining the drift velocity $\vec{v}_D$ as its time averaged velocity for large times.

$$\vec{v}_D := \lim_{t \to \infty} \left(\frac{1}{t} \int_0^t \vec{v}(t) \, \mathrm{d}t \right) \tag{4.24}$$

This tells us in which direction the particle moves on average, while ignoring the specificities of the trajectory. In the unbounded case, $\vec{v}_D$ is the velocity of the escaping particle.

$$\vec{v}_D = \begin{pmatrix} \cos\alpha_+ \\ \sin\alpha_+ \end{pmatrix} = \begin{pmatrix} \sqrt{1 - \frac{1}{\beta^2}} \\ -\frac{1}{\beta} \end{pmatrix} \qquad \text{(for } \beta \geq 1\text{)} \tag{4.25}$$

In the bounded case, $\vec{v}_D$ is the velocity required to Lorentz-boost from the laboratory system into the reference frame in which the particle is (on average) at rest. This is exactly the reference frame with a vanishing electric field, since the magnetic field by itself only produces a periodic trajectory.

$$\vec{v}_D = \begin{pmatrix} 0 \\ -\beta \end{pmatrix} \qquad \text{(for } \beta < 1\text{)} \tag{4.26}$$

The cartesian components of the drift velocity are illustrated as a function of β in Figure 4.5.
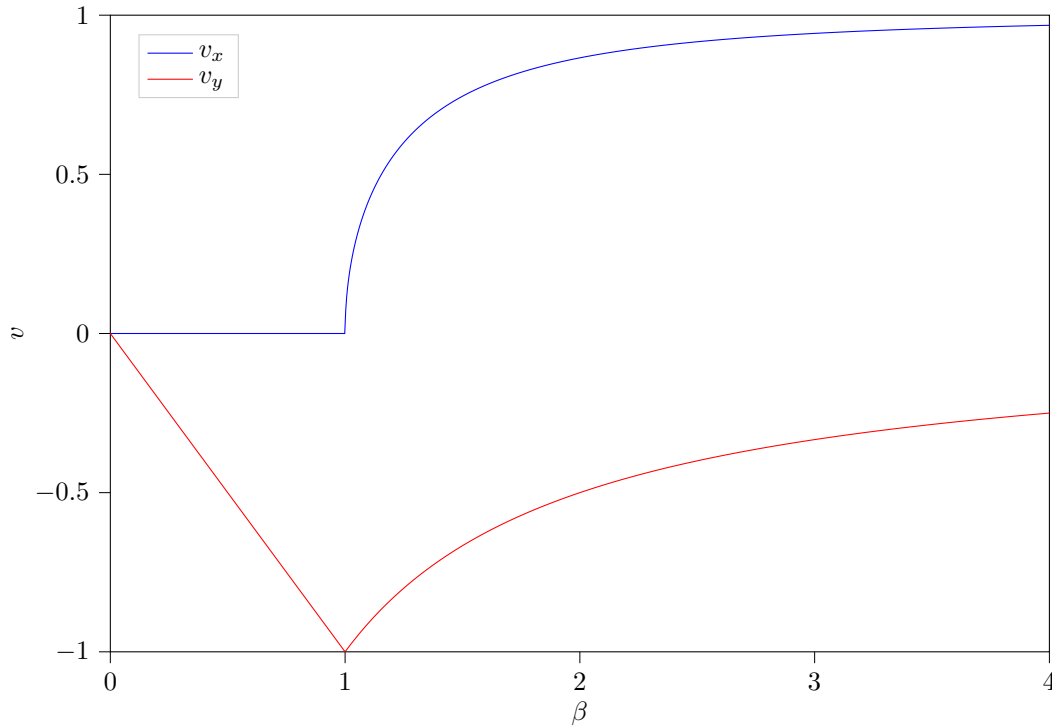

Figure 4.5: Cartesian components of the drift velocity as a function of β, by (4.25) and (4.26)

4.3 Inhomogeneous Electric Field

As a final example, we will consider a case of an inhomogeneous electric field. Specifically, we will choose one whose potential has the form of a hyperbolic tangent function in x. Analytical solutions of quantum equations such as the Dirac and Klein-Gordon equations with this potential have been discussed before [16, 17], but we aim to specifically examine the problem from a semiclassical ultrarelativistic point of view. We can characterize this function with two parameters: let $\delta > 0$ be the absolute potential difference between $\phi(x)$ at $x = \pm\infty$ and $\mathcal{E}_0$ the electric field at $x = 0$. Then, the potential[2] ϕ is given by

$$\phi(x) = -\frac{\delta}{2} \tanh\left(\frac{2\mathcal{E}_0}{\delta} x\right). \tag{4.27}$$

We will now attempt to classify the types of trajectory that can arise from this potential qualitatively. Since analyzing the possible turning points is essential for this undertaking, we again turn our attention to the energy-momentum relation given by (3.12).

$$p_x^2 + (k - \mathcal{B}x)^2 = (E - \phi(x))^2 \tag{4.28}$$

The condition for turning points is $p_x = 0$, which is equivalent to

$$\phi(x) = E - |k - \mathcal{B}x|. \tag{4.29}$$

This means that we can find the turning points by finding the intersections of the function $E - |k - \mathcal{B}x|$ with the potential function. Furthermore, classical motion is only allowed in regions between intersections where $E - |k - \mathcal{B}x| = p - |p_y| + \phi(x)$ is greater than $\phi(x)$, since $p > |p_y|$ must hold.

Reduction of Parameters Considering that the potential is antisymmetric, we can choose $\mathcal{E}_0 > 0$ (meaning $\phi(x)$ is strictly decreasing towards positive x) as well as $\mathcal{B} \geq 0$ without loss of generality. Furthermore, we can make all parameters dimensionless. This is useful for programming the simulations of trajectories and it also removes one degree of freedom from the turning point condition. Additionally, since we will use a graphical approach, dimensionless axes allow us to define angles and lengths on the plane of the graph. We are defining the new parameters as follows.

$$\tilde{E} = \frac{E}{\delta}, \qquad \tilde{\phi} = \frac{\phi}{\delta}, \qquad \tilde{k} = \frac{k}{\delta}, \qquad \tilde{x} = \frac{\mathcal{E}_0}{\delta} x, \qquad \beta = \frac{\mathcal{E}_0}{\mathcal{B}} \tag{4.30}$$

---

[2]The electric field function is then given by $\mathcal{E}(x) = -\phi'(x) = \mathcal{E}_0 \cosh^{-2}\left(\frac{2\mathcal{E}_0}{\delta} x\right)$.

In this new system of units, the potential $\tilde{\phi}$ is given by

$$\tilde{\phi}(\tilde{x}) = -\frac{1}{2}\tanh(2\tilde{x}), \tag{4.31}$$

and we find that the turning point condition (4.29) translates to

$$-\frac{1}{2}\tanh(2\tilde{x}) = \tilde{E} - \left|\tilde{k} - \frac{1}{\beta}\tilde{x}\right| =: f(\tilde{x}). \tag{4.32}$$

Using this equation as a starting point, we now begin the case study. We first characterize $f(\tilde{x})$ as an upside down absolute value function, composed of two linear functions

$$f^-(\tilde{x}) = \tilde{E} - \tilde{k} + \frac{1}{\beta}\tilde{x} \qquad \text{(for } \tilde{x} \leq \beta\tilde{k}), \tag{4.33a}$$

$$f^+(\tilde{x}) = \tilde{E} + \tilde{k} - \frac{1}{\beta}\tilde{x} \qquad \text{(for } \tilde{x} \geq \beta\tilde{k}), \tag{4.33b}$$

meeting at the point $P = (\beta\tilde{k}, \tilde{E})$. To the left of this point, $p_y > 0$ and $f = f^-$ has positive gradient $\frac{1}{\beta}$. Conversely, $f = f^+$ has negative gradient $-\frac{1}{\beta}$ to the right of P, where $p_y < 0$. For ease of explanation, we will call f^- and f^+ the left and right *branches* of f, respectively. Visually, we notice that there are three ways in which f can intersect the potential function: (1) The left and right branches each intersect $\tilde{\phi}$ exactly once, (2) $\tilde{\phi}$ intersects the right branch two times and the left branch not at all, and (3) $\tilde{\phi}$ intersects the left branch once and the right branch three times. A graphical visualization of $\tilde{\phi}$ and f for each of these cases can be seen in Figure 4.6. These cases result in the following qualitative trajectories:

(1) Since $p_y > 0$ and $p_y < 0$ at the left and right turning points, respectively, this motion results in a clockwise looping motion, similar to the bounded case of the homogeneous field. The particle will drift towards negative y because the magnetic field makes it curve away from the left turning point faster (where it has lower momentum) than from the right one (where is has higher momentum), meaning it will spend more time with $p_y < 0$. For future reference, we will refer to this type of trajectory as "loop-like".

(2) In this case, p_y is negative at both turning points and all points in between, meaning that this trajectory will not loop over itself. Qualitatively, we can describe this as "snake-like" motion towards negative y.

(3) In this case we have four turning points. Both qualitative motions (1) and (2) are possible. If the motion is between the first two turning points (left branch and right branch intersection), we have case (1). Else, the motion is between the last two turning points, where we have (2). Motion between the second and third turning points is not possible, since that would mean $f(x) = E - |p_y| < \phi(x)$, i.e. $p < |p_y|$, which is not allowed.
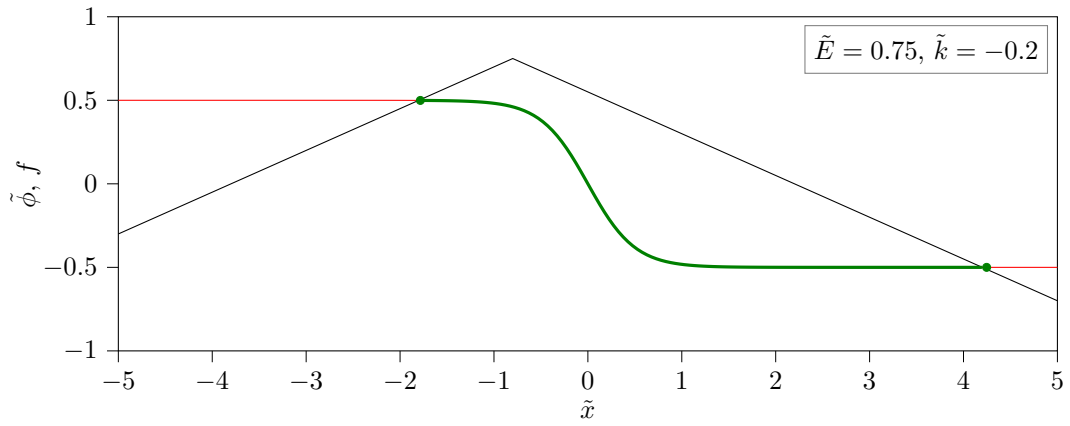
(a) Example of case (1).
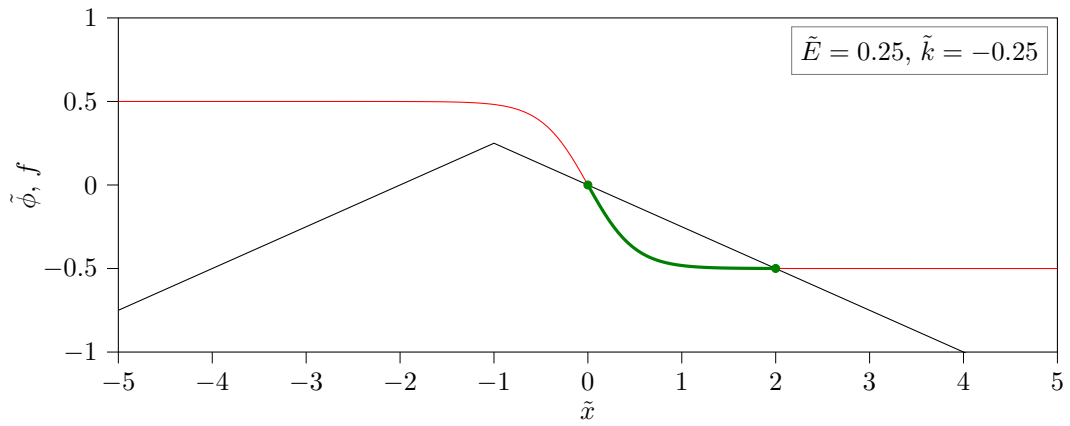
(b) Example of case (2).
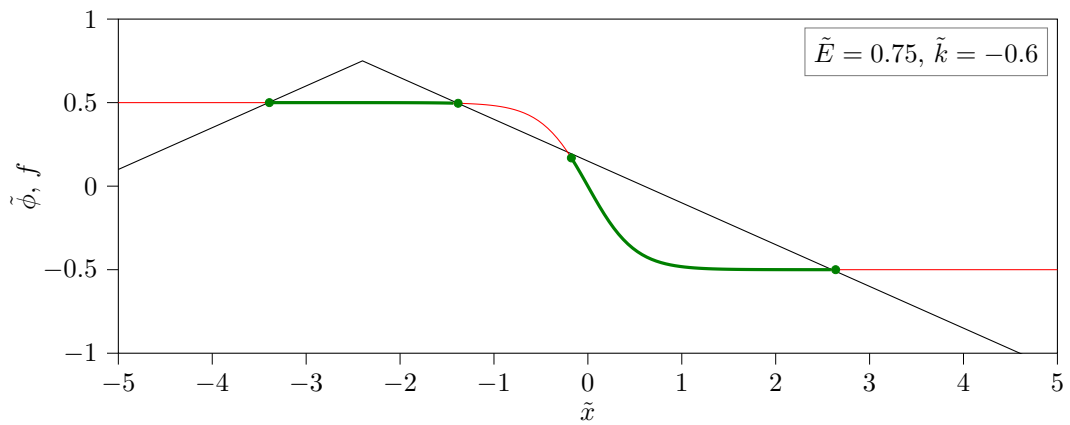
(c) Example of case (3).

Figure 4.6: Examples of the cases for the intersection of f (*black*) and $\tilde{\phi}$ (*green*: allowed regions, *red*: forbidden regions). Parameters: $\beta = 4$; $\tilde{E}$ and $\tilde{k}$ varied (see top right of each plot). Turning points are shown as green dots on the potential function.

Additionally, there are singular limiting cases which mark the boundaries between these three main possibilities and to which we will pay some attention while handling those three main cases. We will now investigate the conditions on the parameters $\tilde{E}$, $\tilde{k}$ and β to obtain each type of motion.

$\boxed{\beta < 1}$:

In this case, the absolute gradient of f^+ is greater than 1, whereas the steepest absolute gradient of $\tilde{\phi}(\tilde{x})$ is 1. Then, by the mean value theorem, the two functions cannot intersect more than once. They also must intersect at least once, since f must be above $\tilde{\phi}(\tilde{x})$ for at least some $\tilde{x}$ and f tends to $-\infty$ towards positive x, whereas $\tilde{\phi}(\tilde{x})$ is bounded by $-\frac{1}{2}$. Therefore, each branch of f intersects $\tilde{\phi}$ exactly once and we have case (1).

$\boxed{\beta = 1}$:

Generally, the same argument as for $\beta < 1$ will hold and this condition will also result in case (1). There is just the boundary case that $\tilde{\phi}$ can be tangential to the right branch of f at the origin. This is the case if and only if f^+ crosses the origin ($\tilde{E} + \tilde{k} = 0$ and $\tilde{k} < 0$). In this case, the particle can oscillate at most one period between the left and right turning points but will approach the right turning point at $x = 0$ without curving back. At the origin, $\beta = 1$ means the electric and magnetic fields are equal, causing a balance of forces and the particle will continue traveling towards negative y in a straight line on $x = 0$.

$\boxed{\beta > 1}$:

In this case, it is possible that the right branch f^+ crosses $\tilde{\phi}$ at most three times. Consider the linear function $g(\tilde{x})$ that has the same gradient as f^+ but a variable y-intercept given by a parameter c.

$$g(\tilde{x}) = c - \frac{1}{\beta}\tilde{x} \tag{4.34}$$

For a given β, we now wish to find the highest possible value c so that g crosses $\tilde{\phi}$ more than once, calling this limit $c_{\max}$. The graph of g will then cross $\tilde{\phi}$ more than once for all $c \in [-c_{\max}, c_{\max}]$ (lower bound by symmetry), as illustrated in Figure 4.7.

It is clear that g is tangential to $\tilde{\phi}$. Let $\tilde{x}_T$ the (leftmost) point at which g and ϕ have the same gradient. A short calculation yields

$$
\begin{aligned}
\tilde{\phi}'(\tilde{x}_T) = g'(\tilde{x}_T) &\Rightarrow -\frac{1}{\cosh^2(2\tilde{x}_T)} = -\frac{1}{\beta} \\
&\Rightarrow \tilde{x}_T = \pm\frac{1}{2}\operatorname{arccosh}\sqrt{\beta} \\
&\Rightarrow \tilde{x}_T = -\frac{1}{2}\operatorname{arccosh}\sqrt{\beta}.
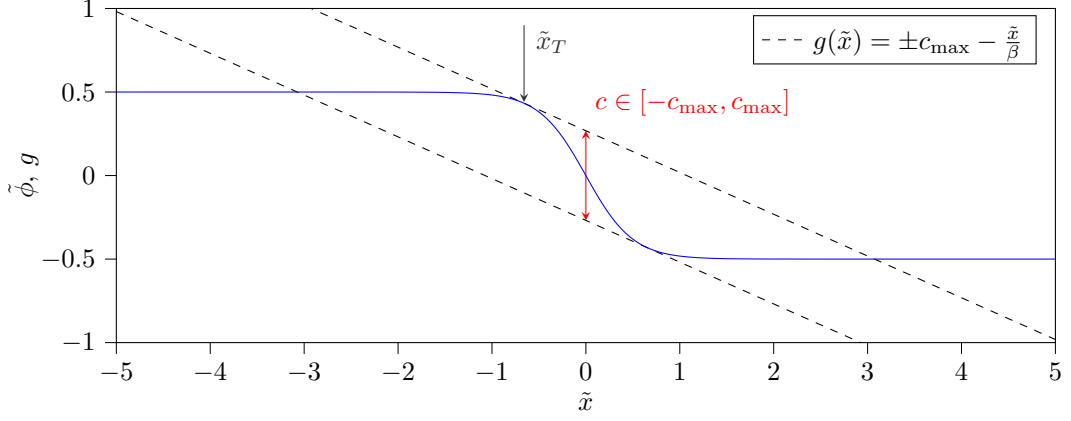\end{aligned}
\tag{4.35}
$$

Figure 4.7: Graphic showing the possible range of the parameter c for which the graph of g crosses the potential $\tilde{\phi}$ (*blue*) more than once. At the extremities, $c = \pm c_{\max}$, the graph of g (*dashed black*) is tangential to $\tilde{\phi}$. Parameter: $\beta = 4$.

The tangent condition is now given by

$$\tilde{\phi}(\tilde{x}_T) = g(\tilde{x}_T), \tag{4.36}$$

from which we may determine the parameter $c_{\max}$.

$$-\frac{1}{2}\tanh(2\tilde{x}_T) = -\frac{1}{\beta}\tilde{x}_T + c_{\max}$$
$$\Rightarrow c_{\max} = \frac{1}{\beta}\tilde{x}_T - \frac{1}{2}\tanh(2\tilde{x}_T) \tag{4.37}$$

Using laws of hyperbolic functions, we can express $\tanh(2\tilde{x}_T)$ in terms of $\cosh(2\tilde{x}_T)$, observing that $\tilde{x}_T$ is negative and hence so is its hyperbolic sine.

$$\tanh(2\tilde{x}_T) = \frac{\sinh(2\tilde{x}_T)}{\cosh(2\tilde{x}_T)} = -\frac{\sqrt{\cosh^2(2\tilde{x}_T) - 1}}{\cosh(2\tilde{x}_T)} \tag{4.38}$$

Substituting this with $\tilde{x}_T$ from (4.35) into (4.37), we obtain

$$c_{\max} = -\frac{1}{2\beta}\operatorname{arccosh}\sqrt{\beta} + \frac{1}{2}\sqrt{\frac{\beta - 1}{\beta}}. \tag{4.39}$$

This implies that for f^+ to cross $\tilde{\phi}$ more than once, the following condition is necessary.

$$|\tilde{E} + \tilde{k}| < c_{\max} = -\frac{1}{2\beta}\operatorname{arccosh}\sqrt{\beta} + \frac{1}{2}\sqrt{\frac{\beta - 1}{\beta}} \tag{4.40}$$

If this condition does not hold, f^+ crosses $\tilde{\phi}$ exactly once, resulting in case (1). If it does hold, then f^+ lies between the two tangents given by $g(\tilde{x}) = \pm c_{\max} - \frac{\tilde{x}}{\beta}$ and we must differentiate the cases

based on the location of the meeting point P, which can lie in one of the four shaded areas (a)–(d) shown in Figure 4.8.
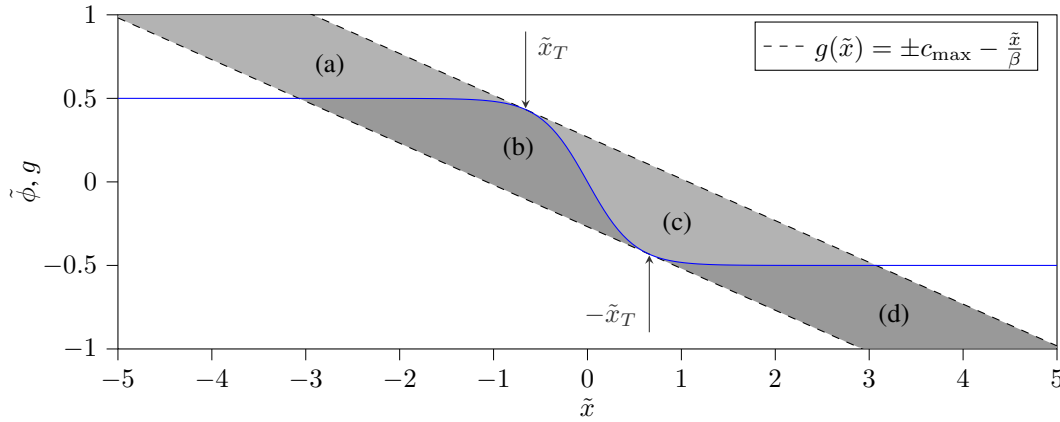

Figure 4.8: Possible locations of the point $P = (\tilde{E}, \beta\tilde{k})$ if $\tilde{E}$ and $\tilde{k}$ fulfill condition (4.40). The electrostatic potential is shown in blue. Parameter: $\beta = 4$.

(a) P is to the left of $\tilde{x}_T$ and above $\tilde{\phi}$.

$$\tilde{k} < -\frac{1}{2\beta}\operatorname{arccosh}\sqrt{\beta}, \qquad \tilde{E} > -\frac{1}{2}\tanh(2\beta\tilde{k}) \tag{4.41}$$

Then f^+ will cross $\tilde{\phi}$ three times, resulting in case (3). For example, see Figure 4.9a.

(b) P is to the left of $-\tilde{x}_T$ and below $\tilde{\phi}$.

$$\tilde{k} < \frac{1}{2\beta}\operatorname{arccosh}\sqrt{\beta}, \qquad \tilde{E} > -\frac{1}{2}\tanh(2\beta\tilde{k}) \tag{4.42}$$

Then f^+ will cross $\tilde{\phi}$ twice, resulting in case (2). For example, see Figure 4.9b.

(c) P is to the right of $\tilde{x}_T$ and above $\tilde{\phi}$.

$$\tilde{k} > -\frac{1}{2\beta}\operatorname{arccosh}\sqrt{\beta}, \qquad \tilde{E} > -\frac{1}{2}\tanh(2\beta\tilde{k}) \tag{4.43}$$

Then f^+ will cross $\tilde{\phi}$ exactly once, resulting in case (1). For example, see Figure 4.9c.

(d) Choices of $\tilde{E}$ and $\tilde{k}$ that do not fulfill any of the above conditions are not allowed, since f would then not cross $\tilde{\phi}$ at all.

If equality holds for any of the above conditions (4.41)–(4.43), i.e. P lies on $\tilde{\phi}$, then P can itself be a turning point, leading to reflection on the potential barrier at that point if it is reached by the particle. This is the limiting case between snake-like and loop-like trajectories.

Furthermore, if equality holds for (4.40), then f can be tangent to $\tilde{\phi}$. In this case the electric and magnetic field are equal at the tangent point, which is then an attractive fixed point in x as described
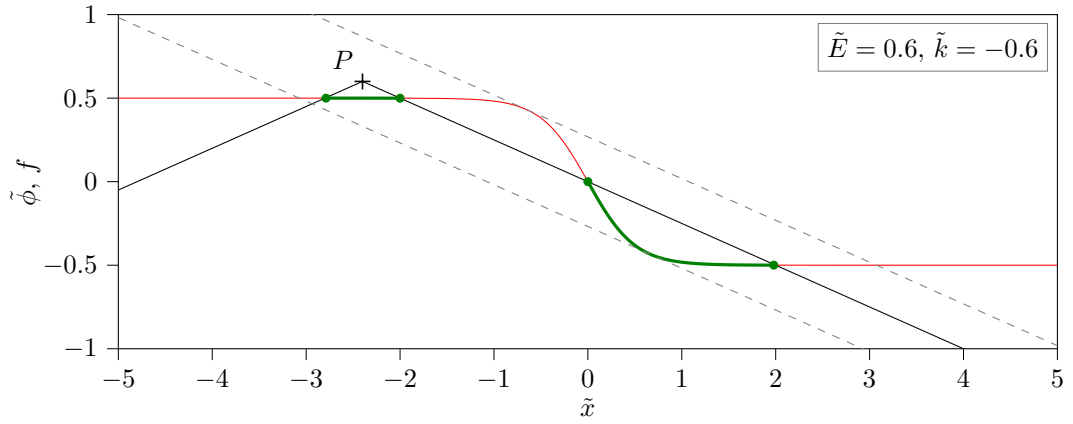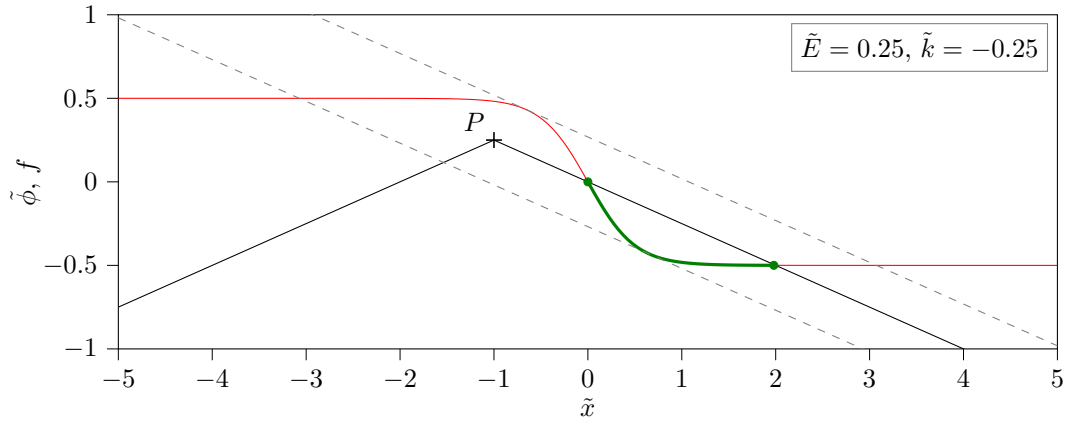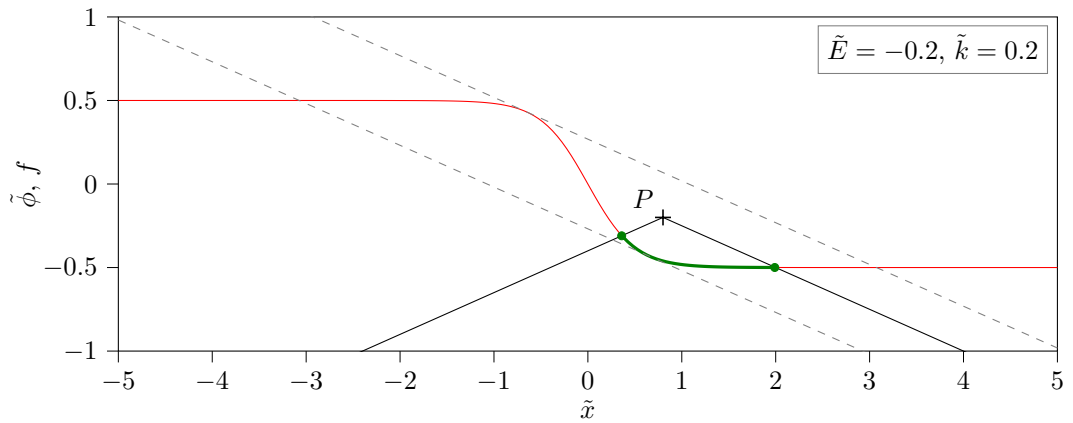
(a) Example of P in area (a).

(b) Example of P in area (b).

(c) Example of P in area (c).

Figure 4.9: Example of locations of $P = (\tilde{E}, \beta\tilde{k})$ fulfilling condition (4.40) leading to three (a), two (b) or one (c) intersection(s) between f^+ (*black*, right of P) and $\tilde{\phi}$ (*green*: allowed regions, *red*: forbidden regions). The tangents on $\tilde{\phi}$ parallel to f^+ are shown in dashed gray. Parameters: $\beta = 4$; $\tilde{E}$ and $\tilde{k}$ varied (see top right of each plot). Turning points are shown as green dots on the potential function.

in the special case $\beta = 1$.

Finally, let us consider the case that there is no magnetic field. In this case $\beta \to \infty$ and our previous calculations are rendered invalid, but we can easily handle this without extensive new calculations. If the magnetic field vanishes, f simply becomes a horizontal line at $\tilde{E}$ above the x-axis. Then it is clear that there is one turning point if $|\tilde{E}| < \frac{1}{2}$, meaning that a particle incoming from positive x will be deflected back towards positive x. Otherwise there is no turning point and the particle will simply move across the entire x-axis.

This concludes the case study of the hyperbolic tangent potential, for which all possible trajectories have been qualitatively categorized. We finish this chapter by showing some examples of the trajectories that can arise in Figure 4.10 and Figure 4.11. These are calculated numerically using the dimensionless equations of motion derived in Appendix A.2.
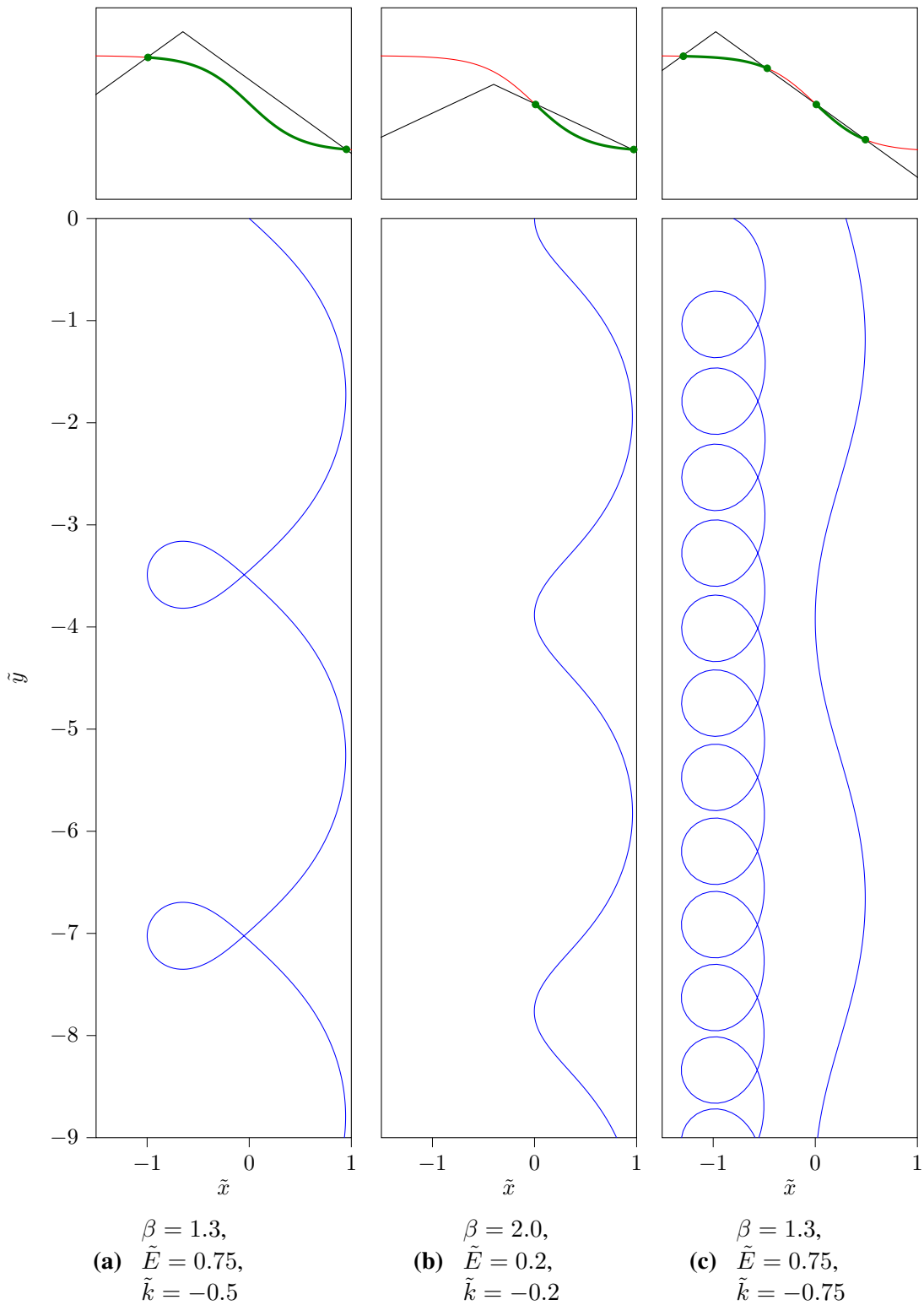
Figure 4.10: Some trajectories for example parameters (*blue*, motion from top to bottom). Above are the graphs showing f, $\tilde{\phi}$ and their intersections on the same x-axis (y-axis arbitrary, colors as in Figure 4.6). The chosen starting points lie on $\tilde{y} = 0$ with various $\tilde{x}$-coordinates. One starting point was chosen for (a) and (b), and two starting points were chosen for (c) to illustrate the two possible types of motion for the same parameters.
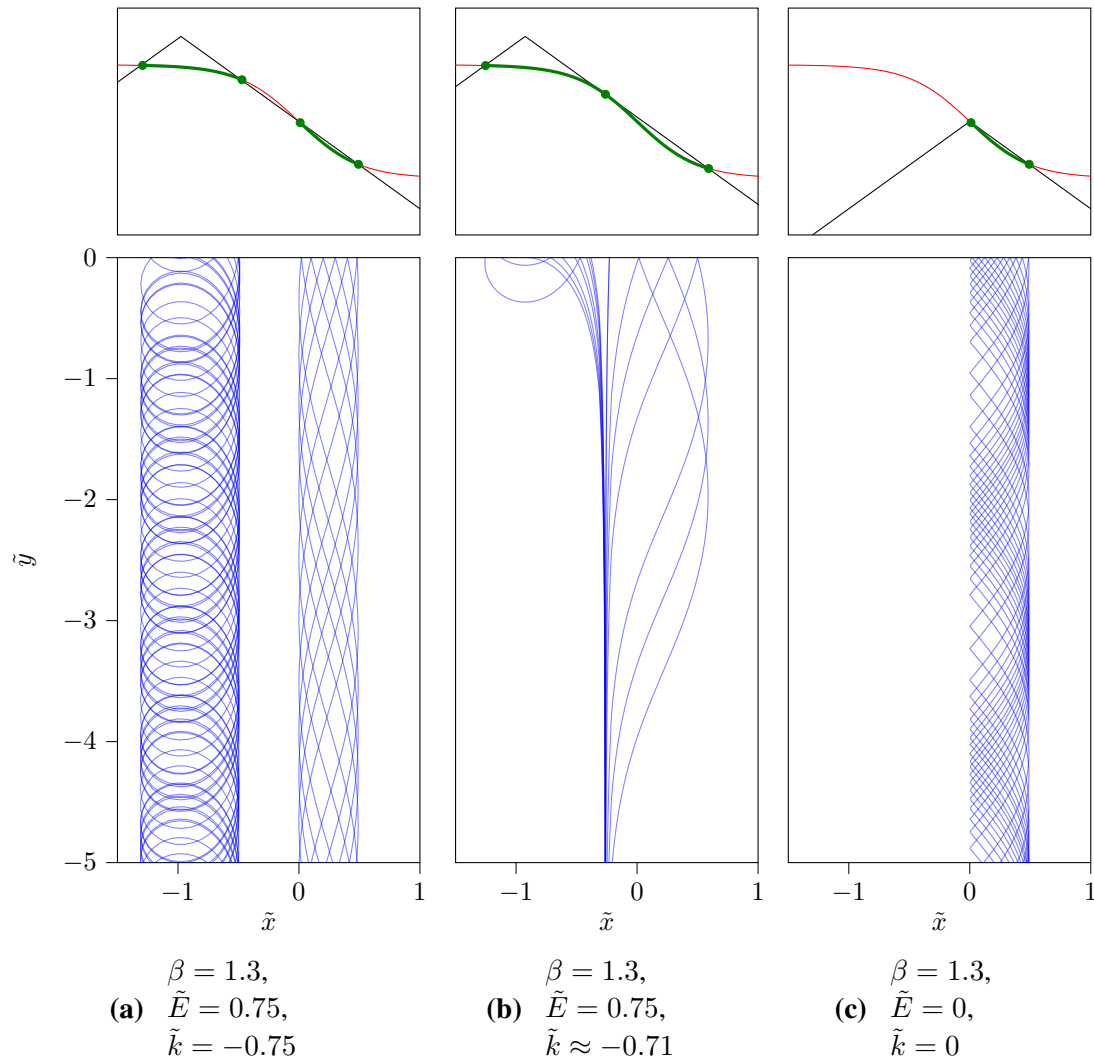
	$\beta = 1.3,$		$\beta = 1.3,$		$\beta = 1.3,$
(a)	$\tilde{E} = 0.75,$	**(b)**	$\tilde{E} = 0.75,$	**(c)**	$\tilde{E} = 0,$
	$\tilde{k} = -0.75$		$\tilde{k} \approx -0.71$		$\tilde{k} = 0$

Figure 4.11: Some trajectories with multiple starting points for example parameters (*blue*, motion from top to bottom). Above are the graphs showing f, $\tilde{\phi}$ and their intersections on the same x-axis (y-axis arbitrary, colors as in Figure 4.6). The chosen starting points lie on $\tilde{y} = 0$ with various $\tilde{x}$-coordinates. (a) Parameters as in Figure 4.10c, showing both loop-like and snake-like motion, (b) Parameters specifically chosen to illustrate the tangent case, in which the particles complete at most one period of oscillation in x before approaching the tangent point, (c) Parameters specifically chosen to illustrate reflection when one turning point is on the electrostatic potential barrier.

5 Conclusion and Outlook

The objective of this work was to examine and categorize trajectories of charge carriers in graphene qualitatively. The focus was on the effect of the electrostatic potential in addition to a homogeneous magnetic field, a setup that can easily be experimentally recreated. Starting from the Dirac equation, we applied the WKB approximation in order to establish a semiclassical energy-momentum relation and the resulting equations of motion, from which we then analyzed specific examples for the electrostatic potential.

Furthermore, we analyzed the behavior of the solutions of the Dirac equation under time-reversal and parity transformations, allowing us to understand the nature of particle-hole symmetry. Since particle-hole pairs can be spontaneously created by external electric fields [18, 19], the examined symmetries can be used to investigate the nature of charge separation within the context of the photoelectric effect.

If the electric field is homogeneous, we found that the trajectories can be well described qualitatively in terms of initial conditions. We were able to categorize the trajectories as unbounded or bounded in x based on the ratio between the electric and magnetic fields and we calculated specific parameters of the motion. Additionally, we discussed the effect of the electrostatic potential barrier as a reflector and investigated the conditions under which it can be reached by a particle.

In the last section, we considered an example of an electric field that is inhomogeneous in one dimension and presented a graphical method of finding the turning points of the motion in x. The method also yields the natural classification of bounded motion as "snake-like" or "loop-like".

There are many ways that the examinations of this work can be developed, the most obvious being to consider other interesting examples for the electrostatic potential. Moreover, the graphical method presented for the inhomogeneous electric field does not yield some parameters that may be considered important, such as the oscillation frequency and the drift speed, both of which are easily calculable in the homogeneous case.

Finally, since the observations made are solely of classical nature, possible quantum effects such as tunneling were ignored. Thus, it may be interesting to examine full solutions of the Dirac equation to investigate the nature of such effects in graphene. For example, Figure 4.11a shows two regions where the particles' motion is either loop-like or snake-like, separated by a gap in which motion is

not classically allowed. However, particles oscillating in one region theoretically have a non-zero probability of tunneling into the other region, which one could investigate further.

A Appendix

A.1 Left Turning Point Calculation for Bounded Trajectories in a Homogeneous Electric Field

In the transformed reference frame, the particle follows a clockwise circular trajectory with radius R. Given that the particle starts in the origin at an angle α_0' (in the transformed system), the circle will be centered in $R(\sin \alpha_0', -\cos \alpha_0')$, meaning that the leftmost x-coordinate is

$$x_{\min} = R(\sin \alpha_0' - 1). \tag{A.1}$$

We already have equation (4.21) for R as a function of α_0 and β, so the task is now to write $\sin \alpha_0'$ in terms of α_0 and β. Using the Lorentz-transformation with $v = -\beta$, we obtain

$$\sin \alpha' = \dot{y}' = \frac{\mathrm{d}y'}{\mathrm{d}t'} = \frac{\beta\gamma \,\mathrm{d}t + \gamma \,\mathrm{d}y}{\gamma \,\mathrm{d}t + \beta\gamma \,\mathrm{d}y} = \frac{\beta + \dot{y}}{1 + \beta\dot{y}} = \frac{\beta + \sin \alpha}{1 + \beta \sin \alpha}. \tag{A.2}$$

Inserting this and (4.21) into (A.1) yields

$$x_{\min} = R_0 \frac{1 + \beta \sin \alpha_0}{1 - \beta^2} \left(\frac{\beta + \sin \alpha_0}{1 + \beta \sin \alpha_0} - 1 \right). \tag{A.3}$$

This simplifies to

$$x_{\min} = R_0 \frac{(\sin \alpha_0 - 1)}{1 + \beta}. \tag{A.4}$$

We can now also prove that this is strictly to the right of the electrostatic potential barrier at $x_B = \frac{R_0}{\beta}$ if $\beta < 1$ (bounded trajectory).

$$\begin{aligned}
\beta < 1 &\Rightarrow \frac{1}{\beta} > 1 \Rightarrow \frac{1}{\beta} > -\sin \alpha_0 \Rightarrow \frac{1 + \beta}{\beta} > 1 - \sin \alpha_0 \\
&\Rightarrow \frac{1}{\beta} > \frac{1 - \sin \alpha_0}{1 + \beta} \Rightarrow -R_0 x_B > -R_0 x_{\min} \Rightarrow x_B < x_{\min}
\end{aligned} \tag{A.5}$$

$\square$

A.2 Dimensionless Equations of Motion

Given the inhomogeneous electrostatic potential

$$\phi(x) = -\frac{\delta}{2}\tanh\left(\frac{2\mathcal{E}_0}{\delta}x\right), \tag{A.6}$$

we can use the following substitutions

$$\tilde{x} = \frac{\mathcal{E}_0}{\delta}x \qquad \left(\frac{\mathrm{d}}{\mathrm{d}\tilde{x}} = \frac{\delta}{\mathcal{E}_0}\frac{\mathrm{d}}{\mathrm{d}x}\right), \tag{A.7a}$$

$$\tilde{y} = \frac{\mathcal{E}_0}{\delta}y, \tag{A.7b}$$

$$\tilde{t} = \frac{\mathcal{E}_0}{\delta}t \qquad \left(\frac{\mathrm{d}}{\mathrm{d}\tilde{t}} = \frac{\delta}{\mathcal{E}_0}\frac{\mathrm{d}}{\mathrm{d}t}\right), \tag{A.7c}$$

$$\tilde{E} = \frac{E}{\delta}, \tag{A.7d}$$

$$\tilde{\phi} = \frac{\phi}{\delta}, \tag{A.7e}$$

$$\beta = \frac{\mathcal{E}_0}{\mathcal{B}}, \tag{A.7f}$$

in the equations of motion (3.29), with which we obtain dimensionless equations of motion.

$$\ddot{\tilde{x}} = \dot{\tilde{y}}\frac{1}{\beta(\tilde{E} - \tilde{\phi}(\tilde{x}))} - \dot{\tilde{y}}^2\frac{\tilde{\phi}'(\tilde{x})}{\tilde{E} - \tilde{\phi}(\tilde{x})}, \tag{A.8a}$$

$$\ddot{\tilde{y}} = -\dot{\tilde{x}}\frac{1}{\beta(\tilde{E} - \tilde{\phi}(\tilde{x}))} + \dot{\tilde{x}}\dot{\tilde{y}}\frac{\tilde{\phi}'(\tilde{x})}{\tilde{E} - \tilde{\phi}(\tilde{x})}, \tag{A.8b}$$

where the dot (˙) means the derivative with respect to $\tilde{t}$ and the prime (′) means the derivative with respect to $\tilde{x}$.

List of Figures

Bibliography

[1] K. S. Novoselov et al., "Electric Field Effect in Atomically Thin Carbon Films", Science **306**, 666–669 (2004).

[2] NobelPrize.org, *The Nobel Prize in Physics 2010*, `https://www.nobelprize.org/prizes/physics/2010/press-release` (visited on 07/07/2021).

[3] K. Lechner, "Electrodynamics of massless charged particles", J. Math. Phys. **56**, 022901 (2015).

[4] M. I. Katsnelson, *The Physics of Graphene*, 2nd ed. (2020).

[5] A. H. Castro Neto et al., "The electronic properties of graphene", Rev. Mod. Phys. **81**, 109–162 (2009).

[6] P. A. M. Dirac, "The quantum theory of the electron", Proc. R. Soc. Lond. A. **117**, 610–624 (1928).

[7] F. J. Ynduráin, *Relativistic Quantum Mechanics and Introduction to Field Theory* (1996).

[8] F. Queisser and R. Schützhold, "Strong Magnetophotoelectric Effect in Folded Graphene", Phys. Rev. Lett. **111**, 046601 (2013).

[9] W. Pauli, "Diracs Wellengleichung des Elektrons und geometrische Optik", Helv. Phys. Acta **5**, 179–199 (1932).

[10] W. Greiner, *Theoretische Physik, Quantenmechanik*, 6th ed., Vol. 3 (2018).

[11] A. D. Kaplan and T. D. Tsankov, "CPT invariance in classical electrodynamics", Eur. J. Phys. **38**, 065205 (2017).

[12] P. A. M. Dirac, "A theory of electrons and protons", Proc. R. Soc. Lond. A. **126**, 360–365 (1930).

[13] L.-J. Yin et al., "Landau quantization of Dirac fermions in graphene and its multilayers", Front. Phys. **12**, 127208 (2017).

[14] W. Wilson, "LXXXIII. The quantum-theory of radiation and line spectra", Lond. Edinb. Dubl. Phil. Mag. **174**, 795–802 (1915).

[15] A. Sommerfeld, "Zur Quantentheorie der Spektrallinien", Ann. Phys. **356**, 1–94 (1916).

[16] C. Rojas, "Scattering of a scalar relativistic particle by the hyperbolic tangent potential", Can. J. Phys. **93**, 85–88 (2015).

[17] A. Suparmi et al., "Solution of D dimensional Dirac equation for hyperbolic tangent potential using NU method and its application in material properties", AIP Conf. Proc. **1710**, 030010 (2016).

[18] R. Schützhold et al., "Dynamically Assisted Schwinger Mechanism", Phys. Rev. Lett. **101**, 130404 (2008).

[19] C. Schneider and R. Schützhold, "Dynamically assisted Sauter-Schwinger effect in inhomogeneous electric fields", J. High Energy Phys. **2016** (2016).

Verfassererklärung / Declaration of Authorship

Hiermit erkläre ich, dass ich diese Arbeit im Rahmen der Betreuung in der Abteilung für theoretische Physik des HZDR und am Institut für theoretische Physik der TU Dresden ohne unzulässige Hilfe Dritter verfasst und alle Quellen als solche gekennzeichnet habe.

I hereby assure that I have produced this work independently under the supervision of the Department of Theoretical Physics of the HZDR and the Institute for Theoretical Physics of the TU Dresden without the help of third parties and have indicated all sources as such.

_____

Joris Josiek

Dresden, 07/2021